AMERICAN METEOROLOGICAL SOCIETY

Bulletin of the American Meteorological Society

EARLY ONLINE RELEASE

The DOI for this manuscript is doi: 10.1175/BAMS-D-15-00221.1

The Green Ocean Amazon Experiment (GoAmazon2014/5) Observes Pollution Affecting Gases, Aerosols, Clouds, and Rainfall over the Rain Forest

Revision 3, "text with low resolution embedded figures.docx". 13193 Words. Submitted: January 2016. Revised: TBD.

S.T. Martin* (1), P. Artaxo (2), L. Machado (3), A.O. Manzi (4), R.A.F. Souza (5), C. Schumacher (6), J. Wang (7), T. Biscaro (3), J. Brito (2), A. Calheiros (3), K. Jardine (8), A. Medeiros (5), B. Portela (4), S.S. de Sá (1), K. Adachi (9), A.C. Aiken (10), R. Albrecht (2), L. Alexander (11), M.O. Andreae (12), H.M.J. Barbosa (2), P. Buseck (13), D. Chand (11), J.M. Comstock (11), D.A. Day (14), M. Dubey (10), J. Fan (11), J. Fast (11), G. Fisch (15), E. Fortner (16), S. Giangrande (7), M. Gilles (8), A.H. Goldstein (17), A. Guenther (18), J. Hubbe (11), M. Jensen (7), J.L. Jimenez (14), F.N. Keutsch (1), S. Kim (18), C. Kuang (7), A. Laskin (11), K. McKinney (1), F. Mei (11), M. Miller (19), R. Nascimento (5), T. Pauliquevis (20), M. Pekour (11), J. Peres (2), T. Petäjä (21), C. Pöhlker (12), U. Pöschl (12), L. Rizzo (20), B. Schmid (11), J.E. Shilling (11), M.A. Silva Dias (2), J.N. Smith (18), J.M. Tomlinson (11), J. Tóta (22), M. Wendisch (23)

Bulletin of the American Meteorological Society

(1) Harvard University, Cambridge, Massachusetts, USA

(2) University of São Paulo, São Paulo, Brazil

(3) National Institute for Space Research, São José dos Campos, Brazil

(4) National Institute of Amazonian Research, Manaus, Amazonas, Brazil

(5) Amazonas State University, Amazonas, Brazil

(6) Texas A&M University, College Station, Texas, USA

(7) Brookhaven National Laboratory, Upton, New York, USA

(8) Lawrence Berkeley National Lab, Berkeley, California, USA

(9) Meteorological Research Institute, Tsukuba, Ibaraki, Japan

(10) Los Alamos National Laboratory, Los Alamos, New Mexico, USA

(11) Pacific Northwest National Laboratory, Richland, Washington, USA

(12) Max Planck Institute for Chemistry, Mainz, Germany

(13) Arizona State University, Tempe, Arizona, USA

(14) University of Colorado, Boulder, Colorado, USA

(15) Aeronautic and Space Institute, São José dos Campos, Brazil

(16) Aerodyne, Inc., Billerica, Massachusetts, USA

(17) University of California, Berkeley, California, USA

(18) University of California, Irvine, California, USA

(19) Rutgers University, New Brunswick, New Jersey, USA

(20) Federal University of São Paulo, São Paulo, Brazil

(21) University of Helsinki, Helsinki, Finland

(22) Federal University of West Para, Santarém, Pará, Brazil

(23) University of Leipzig, Leipzig, Germany

*To whom correspondence should be addressed (scot_martin@harvard.edu)

Capsule

The susceptibility of air quality, weather, terrestrial ecosystems, and climate to human activities was investigated in a tropical environment.

Abstract

The Observations and Modeling of the Green Ocean Amazon (GoAmazon2014/5) experiment took place around the urban region of Manaus in central Amazonia across two years. The urban pollution plume was used to study the susceptibility of gases, aerosols, clouds, and rainfall to human activities in a tropical environment. Many aspects of air quality, weather, terrestrial ecosystems, and climate work differently in the tropics than in the more thoroughly studied temperate regions of Earth. GoAmazon2014/5, a cooperative project of Brazil, Germany, and the USA, employed an unparalleled suite of measurements at nine ground sites and onboard two aircraft to investigate the flow of background air into Manaus, the emissions into the air over the city, and the advection of the pollution downwind of the city. Herein, to visualize this train of processes and its effects, observations aboard a low-flying aircraft are presented. Comparative measurements within and adjacent to the plume followed the emissions of biogenic volatile organic carbon compounds (BVOCs) from the tropical forest, their transformations by the atmospheric oxidant cycle, alterations of this cycle by the influence of the pollutants, transformations of the chemical products into aerosol particles, the relationship of these particles to cloud condensation nuclei (CCN) activity, and the differences in cloud properties and rainfall for background compared to polluted conditions. The observations of the GoAmazon2014/5 experiment illustrate how the hydrologic cycle, radiation balance, and carbon recycling may be affected by present-day as well as future economic development and pollution over the Amazonian tropical forest.

1. Introduction

A magnificent forest two-thirds the size of the continental United States follows the rhythms of the dry and wet seasons in the heart of South America (Salati and Vose 1984; Mares 1986; Garstang et al. 1990; Andreae et al. 2004; Keller et al. 2009; Davidson et al. 2012; Artaxo et al. 2013; ter Steege et al. 2013). The Amazon River, cutting the forest in half latitudinally near the equator, is more than 5 km wide in the narrowest sections during the dry season and expands to widths beyond 100 km, as a river sea, in the widest sections during the wet season. It accounts for about 20% of the world's total flow of fresh water into the ocean. At least several thousand fish species swim in the waters of the Amazon basin, and on the order of 15,000 tree species populate its land. More than several hundred billion trees contribute to its immense carbon inventory.

Within this enormous verdant expanse and excluding coastal urban zones on the margins lies a single major urban metropolitan area, the city of Manaus, meaning "Mother of the Gods" to the indigenous people. Founded by the Portuguese 350 years ago, the present day metropolitan population is more than 2.5 million people. It is located in Amazonas, Brazil, a state of 3.5 million people, which has an area more than twice that of Texas, USA. Manaus is surrounded by undisturbed forest, with small-scale exceptions, for more than 1500 km in all directions upwind and downwind of its emissions.

The history of Manaus is one of boom in the rubber years, complete with the import of European artisans to the "Paris of the Amazon," to bust thereafter, to one of economic revival in recent decades (Grandin 2010). Manaus administered more than 90% of the world's rubber trade in 1900 but less than 5% by 1930, largely as a result of the infamous actions of Englishman Henry Wickham. He surreptitiously transported the rubber seed from the Amazon to the Royal

Botanic Gardens in London, eventually leading to the development of successful rubber plantations in southeast Asia. The reverberations continue today in respect to the rigorous requirements of scientific licenses for foreigners to do research in the Brazilian Amazon. As a consequence of the competition from plantation rubber in Asia, Manaus experienced an economic bust. The downturn was severe and sustained enough across several decades that public electricity was no longer available in Manaus by the 1950s and only the affluent had private generators.

Starting in the 1960s, the ruling military government recognized the Amazon basin as a resource for exploitation and occupation. Manaus was designated as a Free Trade Zone, and plans were developed for dams and long-distance paved roads. This vision has been partially realized in every extent over the past five decades and has guided the political dialogue surrounding the topics of the Amazon forest. Meanwhile, the economy of Manaus has accelerated and flourished again. Its population growth has averaged about 40% every ten years since 1960, and this rapid growth has been associated with equally rapid, though largely unplanned, changes in land use in the region (Figure 1). Today, Manaus is a manufacturing pole within the Brazil economy.

2. GoAmazon2014/5 Motivation

The residential, commercial, and industrial emissions of Manaus, aggregated as a pollution plume and carried westward by the equatorial trade winds, represent a unique laboratory to study the effect of human activities on air quality, weather, terrestrial ecosystems, and climate in a tropical, forested context (Kuhn et al. 2010; Trebs et al. 2012; Bateman et al. 2016; Liu et al. 2016; Martin et al. 2016). Worldwide, no other equivalent large urban area exists that is surrounded in all directions by primary tropical forests for 1500 km and accessed largely

only by boat or plane. The central Amazon in the wet season, absent Manaus, serves as a continental reference of atmospheric properties under background conditions (Andreae 2007), and the opportunity to study the effects of the Manaus plume in this environment represents a unique worldwide reference. At times, there are also episodic intrusions at times of background and polluted Atlantic and African air masses deep into the Amazon (Martin et al. 2010a), and in the dry season regional and continental-scale biomass burning has significant (Artaxo et al., 2002).

The tropical context afforded by Manaus presents a unique and particularly important scientific opportunity. Compared to the temperate zones of Earth, tropical regions have been understudied. Historically, more research has been carried out in economically wealthier parts of the world, which are mostly located in the temperate band of the Northern Hemisphere. The tropics are anticipated to have a special role in the future of global air quality because population growth through 2050 is projected more for the tropical regions of Earth than elsewhere. Furthermore, the energy and hydrological cycles of the tropics, driven by the intense and sustained sunlight across this region, have critical roles in Earth's atmospheric circulation and climate. Any human-induced changes to these cycles can have impacts over the entire Earth. Tropical forests also represent a series of important feedback responses in climate simulations, such as the response of net carbon storage to elevated carbon dioxide, to changed rainfall patterns, and to warmer temperatures, among other factors.

For these reasons, the *Observations and Modeling of the Green Ocean Amazon* (GoAmazon2014/5) experiment was planned for the environs of Manaus. Williams et al. (2002) coined the phrase "Green Ocean" to emphasize the similarities between cloud properties over the Amazon basin during the wet season and those over marine regions. In recent usage, the phrase

has become more generalized to refer to atmospheric properties and processes over the verdant Amazon rain forest. In GoAmazon2014/5, Manaus and the surrounding background region served in combination as a laboratory to assess and understand the effects of human activities on air quality, weather, terrestrial ecosystems, and climate in a tropical context.

3. Experiment Design

Easterlies associated with trade winds normally sweep the urban pollution plume westward. Contours of the modeled frequency distribution of flow trajectories of the Manaus pollution plume, representing a statistical description of flow in each season, are presented in Figure 2. Driven by the easterlies of the trade winds, the plume crosses the river and first intersects the site "T2", which is located just across the Rio Negro. The locations of the research sites around Manaus as well as several associated photos are shown in Figure 3. In the wet season, although the pollution outflow from Manaus most frequently continues southwesterly, 40% of the time it is modeled to go westerly toward the main ground research site "T3". In the dry season, the plume primarily passes westerly from Manaus, and 60% of the time it is modeled to pass over the site "T3". The modeling, however informative, comes with some caveats. Trajectory modeling is based on mean wind fields and as such does not account for vertical and horizontal dispersion of pollutants by turbulent mixing. River breezes, effectively introducing overturning and mixing at the river margins, can occur at fine enough scales that they are not captured by the trajectory modeling.

A Lagrangian design of the surface sites along the plume, including upwind, coupled to aircraft flights in transect to the plume during transport was a powerful and compelling feature of GoAmazon2014/5. The pollution plume was extensively characterized by flights of the G-159 Gulfstream I (G-1) aircraft of the ARM Aerial Facility (AAF) of the USA Department of Energy

(DOE) (Stokes and Schwartz 1994; Mather and Volyes 2013; Schmid et al. 2014). Missions were flown in both the wet and dry seasons. The experiment took place continuously across two years from 1 January 2014 through 31 December 2015, and there were Intensive Operating Periods during the wet and dry seasons of 2014 ("IOP1" and "IOP2", respectively). Research sites and instrumentation of GoAmazon2014/5 are presented in further detail in Martin et al. (2016). In the present account, the first general picture of GoAmazon2014/5 results is presented.

4. Observations

The organization of GoAmazon2014/5 results, as presented herein, follows the origins-to-effect sequence represented in the left panel of Figure 1. In origin, there are natural and anthropogenic emissions of both gaseous compounds and aerosol particles (Martin et al. 2010a). In sequence, important chemical transformations occur for some of the gaseous compounds, ultimately affecting the aerosol particles because of gas-to-particle conversion processes (Martin et al. 2010b). These aerosol particles serve as cloud condensation nuclei (CCN) (Poschl et al. 2010). The physicochemical properties of this CCN population differ significantly between background and polluted conditions (Andreae and Rosenfeld 2008). In net effect, cloud microphysics, droplet size distributions, droplet lifetime, and rainfall can be altered by this sequence of events (Rosenfeld et al. 2008). The large arrow in Figure 1 represents the sweep of these species and associated processes through Manaus and then westward in the prevailing direction of the urban plume across the Rio Negro ("Black River"). Based on measurements obtained from an airborne platform, an informative, interesting, and compelling visualization is presented herein of the pollution plume in the wet season and some of its atmospheric effects over the Green Ocean.

The visualization from the G-1 aircraft of the downwind effects of urban air pollution based on the aircraft measurements is presented in Figures 4 through 7. A revealing crosscut through the complex multi-dimensional data sets of position, time, and measurement type is presented in the following sections. The flight of March 13, 2014, a day of mostly sunny skies and no precipitation along the flight path, serves as a reference.

As an example, the total particle concentrations measured by a condensation particle counter are represented in Figure 4 for transect flights at 500-m altitude in the late morning of March 13. The concentration is plotted in blue in the altitude axis of panel a1. The dominance of the Manaus plume over background conditions is immediately apparent. Transect legs for this flight were separated by approximately 15 min, representing about 1 h of flight time from Manaus to the T3 site. The time for the plume to travel from Manaus to T3 on this day was longer than 3 h according to the trajectory modeling (yellow line). The implication is that the aircraft and the instrumentation onboard sampled the plume much more rapidly than the plume itself was changing. To a first approximation, Figure 4 thus serves as a freeze-frame visualization of the entire plume during the time of the aircraft flight.

4.1 *Gaseous Pollutants and Chemistry*

Several measurements characterizing the pollution plume are plotted in Panel a2 of Figure 4 along the flight path of panel a1. Carbon monoxide (CO), produced during incomplete combustion in vehicles and power plants, and oxides of nitrogen (NO_x), associated with combustion with air as the oxidant, are also plotted in panel a2. CO, NO_x, ozone (O_3), and particulate matter (PM) are important markers of air quality (Unger 2012). NO_x is a reactive species, contributing to net ozone production in the plume. The plot shows that the NO_x concentration decreased along the plume. In addition to loss by entrainment and deposition, NO_x

161 can be chemically transformed into HNO_3 by reaction with OH and to organonitrates by reaction
162 with photochemically produced organic radicals (Perring et al. 2013). By comparison, carbon
163 monoxide can be regarded largely as chemically inert on the timescales of Figure 4. Typically,
164 CO concentration should decrease downwind because of dilution by mixing, entrainment, and
165 other physical processes. For the shown flight data, the CO concentration actually increased by
166 20 ppb with time, providing information about the time course of emissions in Manaus. Up to 5
167 ppb CO is modeled as produced from photooxidation in the plume between Manaus and T3. The
168 flight time of 3000 s over T3 corresponded to 10:55 AM (local), which traces back to rush hour
169 in Manaus at 8 AM. The Manaus emissions of CO added to a background concentration of
170 approximately 80 ppb on this day. Given the estimated atmospheric lifetime of CO of greater
171 than one month, the background concentration has contributions from anthropogenic and
172 biogenic sources both inside and outside of the Amazon basin (Andreae et al. 2012).
173 In addition to the primary emissions (e.g., Figure 4), the pollutants in the plume also have
174 strong secondary effects. Results in Figure 5 for this same late morning, fair weather flight of
175 March 13 demonstrate an accelerated and transformed photochemical cycle. These changes can
176 be attributed to a combination of strong solar irradiance at this equatorial latitude and high
177 concentrations of NO_x within the plume. As a result, the production rate of ozone, a secondary
178 species produced in situ in the atmosphere (Chameides et al. 1988), increased, as seen in its
179 progressive build-up in Figure 5a for plume transects further downwind of Manaus (Sidebar 1).
180 The red line represents the baseline concentrations measured when the aircraft was flying in the
181 background atmosphere outside the plume. The concentrations of the other important
182 atmospheric oxidant, the hydroxyl radical (also a secondary species; Valin et al. (2013)),

183 increased several fold when measured at the T3 ground site during times when the Manaus
184 plume intersected the site under sunny conditions (Sidebar 2).
185 Further indicators of the accelerated oxidant cycle are the decreased BVOC
186 concentrations measured inside relative to outside the plume (e.g., Figure 5b). BVOCs are
187 emitted by the forest, and their concentrations in the boundary layer are a blended effect of
188 emissions rates, reactive loss in the atmosphere, dilution by vertical mixing, and deposition to the
189 planetary surface. Elevated concentrations of hydroxyl radical and ozone increase reactive loss
190 of BVOCs and thereby decrease BVOC concentrations. The effects of this accelerated loss are
191 apparent in Figure 5b. When the aircraft transected the plume the concentration of isoprene,
192 measured onboard the aircraft by a proton-transfer-reaction mass spectrometer, was much lower.
193 Similar results were observed for other BVOCs, such as α-pinene (Figure S1). Corresponding to
194 the loss of the parent species isoprene, its product species were produced. Figure 5c shows the
195 build-up of the ratio of isoprene oxidation products to isoprene. The ratio increased from less
196 than unity to more than two. The ratio increased because of the simultaneous increase in the
197 concentrations of species produced by isoprene oxidation (i.e., methyl vinyl ketone and
198 methacrolein) and decrease in isoprene itself (Figure S1). Benzene and toluene, which are
199 anthropogenic emissions from Manaus, can provide a chemical clock of photochemical age
200 because benzene reacts more slowly than toluene with OH radicals. As a result, the ratio
201 increased downwind from Manaus (Figure 5d). In short, with respect to photochemical aging of
202 gaseous and particulate species by OH radical reaction, the overall changes in Figure 5
203 demonstrate an acceleration of the oxidant cycle by a factor of several fold during the time of the
204 flight. One hour in the pollution plume can be considered equivalent, on a reaction basis, to

several hours in background air on this day, and this phenomenon is referred to as acceleration of the oxidant cycle.

In addition to accelerating the oxidation cycle by increasing OH and O_3, the plume also transformed it. Higher NO concentrations intercepted organic radical species and transformed them into different types of products than form under background conditions (Atkinson 1990; Atkinson and Arey 2003; Liu et al. 2013; Liu et al. 2016). Species such as organic hydroperoxides were replaced by species such as organonitrates, among others (Farmer et al. 2010). The organic PM in the plume had contributions both from the primary emissions of Manaus as well as from secondary processing tied to gas-to-particle partitioning in the accelerated chemistry of the plume. Although difficult to observe directly using the instrumentation onboard the G-1, this suite of additional chemical changes was recorded by more extensive analytical instrumentation deployed at the ground sites (results not shown herein) (Isaacman-VanWertz et al. 2016).

4.2 *Particulate Matter Number Concentrations*

The concentration of particles in the center of the plume approached 30,000 cm^{-3} (STP), compared to <500 cm^{-3} under background conditions (panel a2, top row). The gray and black lines correspond to concentrations of particles having diameters greater than 3 and 10 nm, respectively, denoted by $N_{>3}$ and $N_{>10}$ hereafter. The difference between $N_{>3}$ and $N_{>10}$ shows the importance of nanoparticles in the Manaus plume, believed to be largely derived from new particle production associated with combustion emissions. The difference between $N_{>3}$ and $N_{>10}$ became negligible sufficiently downwind, indicating the absence of the smallest particles by that point. The decrease in concentration of both $N_{>3}$ and $N_{>10}$ with flight time, representing further downwind from Manaus, arose from a combination of coagulation, dilution from vertical

entrainment of clean air, dilution from horizontal dispersion, and dry deposition. There was no precipitation along the flight path on this day, which otherwise can decrease particle concentration by wet deposition and deep convection.

The transects across the plume were complemented in a moment of real-time in-flight excitement when the flight scientist identified the location of the plume and then directed the aircraft to follow a flight course directly up the central axis of the plume. The results are plotted in the lower row of Figure 4 as panels b1 and b2. The interpretation of these panels must be considered with some care because the flight leg and the central axis of the plume are somewhat askew of one another, and the concept of a central axis for the plume is somewhat fictitious in the dynamical setting of winds, entrainment, and dispersion. Even so, the visualization in panel b1 of the axial flight clearly conveys the idea of plume extending from Manaus, in which particle number concentrations decrease with distance. The top row of panel b2 shows this decrease more quantitatively, as concentrations decreased from 35,000 cm^{-3} to 10,000 cm^{-3} in the transit from Manaus to T3 during this flight.

Although the data in panel b2 reflect a clear trend in particle concentrations, undulations on the order of ±20% are also apparent. These undulations can arise from a combination of processes. Early in the plume, heterogeneous emissions throughout Manaus from specific power plants and industrial areas contribute to variability of species concentrations in the plume. Later in the plume, differing amounts of vertical entrainment from the overlying free troposphere, a stochastically governed process, have taken place, and this entrained air has lower concentrations of the pollutants. A comparison to the data sets for CO and NO_x in the middle and lower rows of panel b2 provides some further insight into the relative contribution of these processes. Early in the plume, CO concentrations had less variability, suggesting that non-points sources, such as the

transportation fleet of Manaus, represented the dominant source of this pollutant. By comparison, NO_x concentrations had relatively high variability, suggesting that point sources, such as power plants, strongly contributed to the concentrations of this pollutant. The particle count had tendencies of both, suggesting that both the transportation fleet (which has many diesel trucks to accompany the activities of the factories associated with the Free Trade Zone) and power plants had significant particle emissions. At later times (500 to 900 s, panel b2, nearby T3), undulations remain apparent in the measurements, despite the mixing tendencies associated with dilution, entrainment, and other aspects of turbulence, such as large eddies. The implication is that on this day specific lines of pollution within the plume maintained their integrity to a certain extent over the distance from Manaus to T3, implying that horizontal dispersion was rather weak and air parcels underwent quasi-Lagrangian transport from emission to observation, at least on this fair weather day. Another observation is that the CO and NO_x concentrations at 800 s in panel b2 are lower than their respective maximum values at 3000 s in panel a2. Askewness between the flight path and the central axis of the plume can explain this observation, meaning that at 800 s the flight path was sampling the shoulder rather than the central values of the plume.

4.3 *Cloud Condensation Nuclei*

The cloud-forming characteristics of the atmospheric PM were also altered by the pollution plume. For the flight on March 13, the concentrations of particles activating as cloud droplets were 80 and 130 cm^{-3} outside the plume for supersaturations of 0.23% and 0.50%, respectively (labeled $CCN_{0.23}$ and $CCN_{0.50}$; Figures 6a and 6b). These supersaturations are typically achieved as maximum in-cloud supersaturations across the range of moderate to strong convection. By comparison, $CCN_{0.23}$ and $CCN_{0.50}$ shifted to values greater than 300 and 600 cm^{-3}, respectively, in the central region of the pollution plume. Cloud microphysics is most

sensitive to changes in CCN number concentrations from 100 to 1000 cm^{-3}, above which saturation effects occur (Reutter et al. 2009).

The increased CCN concentrations associated with the pollution plume can be partially attributed to changes in particle size (i.e., physics) as well as changes in intrinsic CCN activity (i.e., chemistry). The particles freshly emitted in Manaus, mostly smaller than 50 nm and having a high soot content, were both too small and too hydrophobic to serve favorably as CCN. Downwind, the particle number concentration decreased, in part because of nanoparticle coagulation, as discussed for Figure 4. Coagulation, as well as condensation of gases onto preexisting particles, increased the population of particles 100 nm and larger. Large particles tend to activate as CCN even at low supersaturations. Condensing gases are also produced more rapidly in the accelerated oxidant cycle of the pollution plume. The condensing gases include relatively hygroscopic species, such as carboxylic acids, alcohols, hydroperoxides, or sulfuric acid, resulting in particles of higher intrinsic CCN activity when condensational growth occurs. The CCN concentration thus progressively increased downwind of Manaus, both because of physics (i.e., mode diameter shifted to larger sizes) and chemistry (i.e., more hygroscopic constituents).

The effects of the plume on the downwind CCN concentrations are shown in Figures 6c, 6d, and 6e for the flight of March 13. The number concentration measured by the Passive Cavity Aerosol Spectrometer Probe (PCASP) instrument, sensitive to particle diameters of 100 nm and larger (labeled $N_{>100}$), steadily increased further downwind within the plume (Figure 6c), even as total particle number concentrations $N_{>3}$ and $N_{>10}$ decreased (panel a2, Figure 4), indicating a shift of the particle population to a larger mode diameter. Because of the large diameters, most of these particles activated at 0.23% supersaturation, as reflected in the ratio of $CCN_{0.23}/N_{>100}$ in

297 Figure 6d, which mostly varied from 0.5 to 0.8 for this flight. Even so, these CCN-active
298 particles remained a small fraction of the total particle population ($CCN_{0.23}/N_{>10}$, Figure 6e). This
299 ratio was nearly zero in the plume and about 0.2 for background conditions. The ratio
300 $CCN_{0.23}/N_{>100}$ was typically lower inside the pollution plume. A shift in the relative size
301 distribution of particles of diameters 100 nm and larger (i.e., to a smaller mode diameter) and a
302 decrease in their hygroscopicity, both of which are associated with dominance of small
303 hygroscopic particles in the plume, are both factors that can explain the decrease in
304 $CCN_{0.23}/N_{>100}$.

305 To a limited extent, the pollution plume also changed the thermodynamic context of
306 cloud formation in important ways. The PM observed during background conditions for this
307 flight had a high single-scattering albedo of 0.95 or larger but blackened considerably in the
308 plume, approaching a single-scattering albedo of 0.75 or less in the center of the plume
309 (Supplementary Figure S2). Light absorption causes a redistribution of energy in the atmospheric
310 column, having a general tendency to increase atmospheric stability, decrease entrainment of
311 overlying clean air, and weaken the environment for development of shallow clouds (Jacobson
312 2001).

313 4.4 *Cloud Properties*

314 In light of changes both in CCN concentrations and possibly increased atmospheric
315 stability at times because of absorption by black carbon, cloud properties in regions affected by
316 the Manaus plume can be anticipated to change significantly. Even so, predictions of detailed
317 effects on cloud formation are challenging because of myriad interacting factors, including but
318 not limited to CCN concentrations, updraft velocity, temperature, and humidity (Andreae and
319 Rosenfeld 2008). The observations made in GoAmazon2014/5, however, provide both

qualitative descriptions and quantitative constraints of the effects of the pollution plume on cloud properties.

As an example, the droplet size distribution, meaning the probability density function of number concentration with diameter, is one important cloud property, affecting both cloud albedo as well as the tendency to convert from a non-precipitating to precipitating state. Droplet size distributions were recorded when the aircraft passed through shallow cumulus clouds. The main reference day of March 13 presented herein had mostly sunny skies, and the aircraft passed through hardly any clouds. Instead, data sets of March 19 and 21, corresponding to the same latitude-longitude box downwind of Manaus and about the same altitude (600 m asl), just above cloud base, were used in the analysis. The meteorological conditions such as temperature, relative humidity, and cloud vertical velocity were also similar for the two data sets. On March 21, the Manaus pollution plume blanketed the selected latitude-longitude box. On March 19, the Manaus pollution plume was outside this box. On both days, the flights passed through shallow cumulus clouds.

The CCN concentrations observed on March 19 (background conditions; blue color) and March 21 (polluted conditions; red color) are shown in the top panel of Figure 7 for 0.35% supersaturation. Under background conditions, $CCN_{0.35}$ was approximately 100 cm^{-3} for both flights. It increased to 400 to 800 cm^{-3} inside the plume for the flight of March 21. These observations are similar to those previously described for the main reference day of March 13 (cf. Figure 6). The bottom panel of Figure 7 shows the size distributions, spanning droplets to raindrops, measured for the clouds under polluted and background conditions. The distributions differed considerably. Under polluted conditions, the droplet size distribution shifted to significantly smaller diameters, as explained by the increased CCN concentration. The dispersion

of the distribution also decreased. The concentration of small droplets (< 10 μm) increased by up to two orders of magnitude in the polluted clouds. Raindrop concentrations (> 100 μm) correspondingly decreased significantly. Even so, caveats to keep in mind are that cloud formation mechanisms could differ between the days and possible meteorological effects cannot be disentangled beyond doubt from possible effects of pollution. These caveats notwithstanding, the comparison between shallow cumulus clouds on these days is as reasonably similar as possible. In a broader statistical evaluation of clouds inside and outside the plume in the wet season, Cecchini et al. (2016) report similar findings. The differing size distributions suggest that the Manaus pollution plume has the general effect of slowing collision-coalescence processes of shallow cumulus clouds, thereby reducing droplet sizes and delaying or suppressing the formation of raindrops.

4.5 *Precipitation*

Differences in the droplet size distributions under polluted compared to background conditions can influence the timing, amount, and intensity of rainfall, at least for some thermodynamic settings. Gonçalves et al. (2015) used observational evidence over the Manaus region to connect increased ice content, rain cells, and ultimately precipitation to elevated concentrations of atmospheric particles derived from biomass burning. The smaller mode diameters of the droplet size distributions during cloud development under polluted conditions can suppress early-stage precipitation within warm regions of the clouds. Liquid particles can rise to higher altitudes where freezing occurs, which is typically above 5 km over the Amazon. The latent heat of fusion promotes stronger updrafts and the growth of large ice particles, eventually leading to enhanced rainfall. This aerosol-cloud-precipitation mechanism is important

365 in many environments (Khain et al. 2005; Rangno and Hobbs 2005; Rosenfeld et al. 2008; Fan et
366 al. 2012).

367 As an illustration of these topics, Figure 8 shows vertical distributions for the frequency
368 of occurrence of radar reflectivity, commonly referred to as a Contoured Frequency by Altitude
369 Diagram (CFAD). The data were collected at T3 during the wet season using a dual polarization
370 X-band scanning radar in a vertical pointing strategy. Warmer colors represent a higher
371 frequency of occurrence at a particular altitude, and the sum of occurrence at each height equals
372 100%. The top and bottom panels represent data aggregated into polluted and background
373 conditions, respectively. The two data sets respectively aggregate 1680 and 881 observations of
374 10 min each. The polluted or background classification is based on a conglomeration of physical
375 and chemical measurements at T3, such as particle number, CCN, and NO_x concentrations.
376 Although environmental controls on cloud development are complex, even more so for a single
377 cloud, broad aggregation over an extended dataset of many clouds and many days has the
378 possibility to make a statistical comment regarding factors of influence, such as polluted
379 compared to background conditions, on the effects of the Manaus plume on cloud development
380 in the wet season.

381 In this regard, the CFAD analysis represented in Figure 8 illustrates altered cloud
382 properties associated with the pollution plume of Manaus in the wet season. The horizontal line
383 at 5 km represents the typical height of the melting layer over the Amazon, below which warm
384 rain processes are normally active. The vertical lines draw attention to a window of 15 to 20 dBZ
385 in radar reflectivity. Clouds both above and below the melting layer are associated with a wider
386 spread in reflectivity for polluted compared to background conditions. Below the melting layer,
387 the wide spread in reflectivity suggests larger rainfall rates, larger mean drop sizes, or both.

Above the melting layer, the high-end tail of the wide spread in reflectivity suggests that graupel and other mixed-phase hydrometeors are larger, more numerous, or both under polluted conditions. The aforementioned aerosol-cloud-precipitation mechanism can explain the enhanced ice content under polluted conditions.

Given the myriad influences on rainfall occurrence and intensity, the most challenging analysis is to investigate the possible effect of the Manaus pollution plume on these outcomes. Disdrometer measurements at the T3 site are shown in Figure 9. The rain rate and the mean mass-weighted diameter of the falling hydrometeors are measured. Figure 9 segregates the data for polluted compared to background conditions. The mean diameters of the two populations are not statistically different (1.5 mm), and the mean rain rates are not too different (6.4 and 7.5 mm h^{-1} for background and polluted conditions, respectively). For most cases, then, the overall precipitation distributions are not significantly different. A focus on strong rain rates, however, modifies the interpretation. For rain rates larger than 20 mm h^{-1} that denote deep convection, the mean diameter is larger for polluted conditions. The positive skewness representing the tail to larger diameters in the droplet distribution for the polluted compared to background conditions is statistically significant by Student's t-test to greater than 95% confidence. The implication appears to be that in the mixture of influences that affect rainfall occurrence and intensity at times pollution can play a role in shifting the kinematic and microphysical growth processes. At those times, the shift to larger rain drops is consistent with the aerosol-cloud-precipitation mechanism of invigoration (May et al. 2011).

5. Final Words

In closing perspective, just before the dawn of World War I, the Roosevelt-Rondon Scientific Expedition of 1913-14 took place up a deep tributary in southwestern Amazonia, and

Theodore Roosevelt (President, USA, 1901-1909) published thereafter *Through the Brazilian Wilderness*. In reference to the forest, he states that "decades will pass before it vanishes," by which he meant logging and other forms of development. In the most recent ten years, a little over 2% of the forest has vanished. Tellingly, in 2015, acrid and thick smoke formed a pall across Manaus more often than not through October and November of the late dry season. Lifetime residents recall no other year as such. Although an El Niño year has been brought up as explanation, many El Niño years have come in the past without these fires, and in fact the quantitative incidence of fires in and around Manaus has increased steadily over the past 10 years at an annual average growth rate of 20%. Possibly, 2015 is a harbinger of future years and could mark a major change in terms of fire location from the historical arc of deforestation along the southern margins of the Amazon forest and now into the central Amazon basin as well.

The results of GoAmazon2014/5 are improving understanding of the scientific factors affecting air quality, weather, terrestrial ecosystems, and climate in the basin, especially as related to susceptibility to specific human factors. A positive legacy will be that future regional development will take into account what is learned from GoAmazon2014/5 when making choices about future transportation networks, energy matrices, land-use changes, and other pertinent factors. In addition to the recent technical introduction by Martin et al. (2016) to the GoAmazon2014/5 experiment, several overview papers focused on more specific topics are forthcoming in *Atmospheric Chemistry and Physics* to summarize and synthesize findings concerning the aerosol life cycle, the cloud life cycle, and cloud-aerosol-precipitation interactions, in particular their functioning under background conditions compared to times of direct human influence.

Acknowledgments. Institutional support was provided by the Central Office of the Large Scale Biosphere Atmosphere Experiment in Amazonia (LBA), the National Institute of Amazonian Research (INPA), the National Institute for Space Research (INPE), Amazonas State University (UEA), and the Brazilian Space Agency (AEB). The Office of Biological and Environmental Research of the Office of Science of the United States Department of Energy is acknowledged for funding, specifically the Atmospheric Radiation Measurement (ARM) Climate Research Facility, the Atmospheric System Research (ASR) Program, the Terrestrial Ecosystem Sciences (TES) Program, the Regional & Global Climate Modeling (RGCM) Program, and the Environmental Molecular Sciences Laboratory (EMSL). Further funding was provided by the Amazonas State Research Foundation (FAPEAM), the São Paulo State Research Foundation (FAPESP), the Brazil Scientific Mobility Program (CsF/CAPES), the United States National Science Foundation (NSF), the German Max Planck Society (MPG), the German Research Foundation (DFG), and the German Aerospace Center (DLR). The work was conducted under scientific licenses 001030/2012-4, 001262/2012-2, and 00254/2013-9 of the Brazilian National Council for Scientific and Technological Development (CNPq). We thank Karla M. Longo for her leadership related to the G-1 aircraft as part of GoAmazon2014/5.

References

Andreae, M. O., 2007: Aerosols before pollution. *Science*, **315,** 50-51, 10.1126/science.1136529.

Andreae, M. O., and D. Rosenfeld, 2008: Aerosol cloud precipitation interactions. Part 1. The nature and sources of cloud-active aerosols. *Earth Science Reviews*, **89,** 13-41, 10.1016/j.earscirev.2008.03.001.

Andreae, M. O., D. Rosenfeld, P. Artaxo, A. A. Costa, G. P. Frank, K. M. Longo, and M. A. F. Silva-Dias, 2004: Smoking rain clouds over the Amazon. *Science*, **303,** 1337-1342, 10.1126/science.1092779.

Andreae, M. O., P. Artaxo, V. Beck, M. Bela, S. Freitas, C. Gerbig, K. Longo, J. W. Munger, K. T. Wiedemann, and S. C. Wofsy, 2012: Carbon monoxide and related trace gases and aerosols over the Amazon Basin during the wet and dry seasons. *Atmos. Chem. Phys.*, **12,** 6041-6065, 10.5194/acp-12-6041-2012.

Andreae, M. O., O. C. Acevedo, A. Araùjo, P. Artaxo, C. G. G. Barbosa, H. M. J. Barbosa, J. Brito, S. Carbone, X. Chi, B. B. L. Cintra, N. F. da Silva, N. L. Dias, C. Q. Dias-Júnior, F. Ditas, R. Ditz, A. F. L. Godoi, R. H. M. Godoi, M. Heimann, T. Hoffmann, J. Kesselmeier, T. Könemann, M. L. Krüger, J. V. Lavric, A. O. Manzi, A. P. Lopes, D. L. Martins, E. F. Mikhailov, D. Moran-Zuloaga, B. W. Nelson, A. C. Nölscher, D. Santos Nogueira, M. T. F. Piedade, C. Pöhlker, U. Pöschl, C. A. Quesada, L. V. Rizzo, C. U. Ro, N. Ruckteschler, L. D. A. Sá, M. de Oliveira Sá, C. B. Sales, R. M. N. dos Santos, J. Saturno, J. Schöngart, M. Sörgel, C. M. de Souza, R. A. F. de Souza, H. Su, N. Targhetta, J. Tóta, I. Trebs, S. Trumbore, A. van Eijck, D. Walter, Z. Wang, B. Weber, J. Williams, J. Winderlich, F. Wittmann, S. Wolff, and A. M. Yáñez-Serrano, 2015: The Amazon Tall Tower Observatory (ATTO): overview of pilot measurements on ecosystem ecology, meteorology, trace gases, and aerosols. *Atmos. Chem. Phys.*, **15,** 10723-10776, 10.5194/acp-15-10723-2015.

Artaxo, P., L. V. Rizzo, J. F. Brito, H. M. J. Barbosa, A. Arana, E. T. Sena, G. G. Cirino, W. Bastos, S. T. Martin, and M. O. Andreae, 2013: Atmospheric aerosols in Amazonia and land use change: from natural biogenic to biomass burning conditions. *Faraday Discussions*, **165,** 203, 10.1039/c3fd00052d.

Atkinson, R., 1990: Gas-phase tropospheric chemistry of organic compounds: a review. *Atmospheric Environment*, **24,** 1-41, 10.1016/j.atmosenv.2007.10.068.

Atkinson, R., and J. Arey, 2003: Gas-phase tropospheric chemistry of biogenic volatile organic compounds: a review. *Atmos. Environ.*, **37,** 197-219, 10.1016/S1352-2310(03)00391-1.

Bateman, A. P., Z. Gong, P. Liu, B. Sato, G. Cirino, Y. Zhang, P. Artaxo, A. K. Bertram, A. O. Manzi, L. V. Rizzo, R. A. F. Souza, R. A. Zaveri, and S. T. Martin, 2016: Sub-micrometre particulate matter is primarily in liquid form over Amazon rainforest. *Nature Geosci*, **9,** 34-37, 10.1038/ngeo2599.

Cecchini, M. A., L. A. T. Machado, J. M. Comstock, F. Mei, J. Wang, J. Fan, J. M. Tomlinson, B. Schmid, R. Albrecht, S. T. Martin, and P. Artaxo, 2016: Impacts of the Manaus pollution plume on the microphysical properties of Amazonian warm-phase clouds in the wet season**,** submitted. *Atmos. Chem. Phys.*, in press.

Chameides, W., R. Lindsay, J. Richardson, and C. Kiang, 1988: The role of biogenic hydrocarbons in urban photochemical smog: Atlanta as a case study. *Science*, **241,** 1473-1475, 10.1126/science.3420404.

Davidson, E. A., A. C. de Araújo, P. Artaxo, J. K. Balch, I. F. Brown, M. M. C. Bustamante, M. T. Coe, R. S. DeFries, M. Keller, M. Longo, J. W. Munger, W. Schroeder, B. S. Soares-Filho, C. M. Souza, and S. C. Wofsy, 2012: The Amazon basin in transition. *Nature*, **481,** 321-328, 10.1038/nature10717.

May, P. T., V. N. Bringi, and M. Thurai, 2011: Do we observe aerosol impacts on DSDs in strongly forced tropical thunderstorms? *J. Atmos. Sci.*, **68**, 1902-1910, dx.doi.org/10.1175/2011JAS3617.1.

Fan, J., D. Rosenfeld, Y. Ding, L. R. Leung, and Z. Li, 2012: Potential aerosol indirect effects on atmospheric circulation and radiative forcing through deep convection. *Geophys. Res. Lett.*, **39,** n/a-n/a, 10.1029/2012gl051851.

Farmer, D. K., A. Matsunaga, K. S. Docherty, J. D. Surratt, J. H. Seinfeld, P. J. Ziemann, and J. L. Jimenez, 2010: Response of an aerosol mass spectrometer to organonitrates and organosulfates and implications for atmospheric chemistry. *Proc. Natl. Acad.*, **107,** 6670-6675, 10.1073/pnas.0912340107.

Freitas, S. R., K. M. Longo, M. A. F. Silva Dias, R. Chatfield, P. Silva Dias, P. Artaxo, M. O. Andreae, G. Grell, L. F. Rodrigues, A. Fazenda, and J. Panetta, 2009: The Coupled Aerosol and Tracer Transport model to the Brazilian developments on the Regional Atmospheric Modeling System (CATT-BRAMS) – Part 1: Model description and evaluation. *Atmos. Chem. Phys.*, **9,** 2843-2861, 10.5194/acp-9-2843-2009.

Garstang, M., S. Greco, J. Scala, R. Swap, S. Ulanski, D. Fitzjarrald, D. Martin, E. Browell, M. Shipman, V. Connors, R. Harriss, and R. Talbot, 1990: The Amazon Boundary-Layer Experiment (ABLE 2B): A Meteorological Perspective. *B. Am. Meteorol. Soc.*, **71,** 19-32, 10.1175/1520-0477(1990)071<0019:TABLEA>2.0.CO;2.

Gonçalves, W. A., L. A. T. Machado, and P. E. Kirstetter, 2015: Influence of biomass aerosol on precipitation over the Central Amazon: an observational study. *Atmos. Chem. Phys.*, **15,** 6789-6800, 10.5194/acp-15-6789-2015.

Grandin, G., 2010: *Fordlandia: The Rise and Fall of Henry Ford's Forgotten Jungle City.* Picador.

Isaacman-VanWertz, G., L. D. Yee, N. M. Kreisberg, R. Wernis, J. A. Moss, S. V. Hering, S. S. d. Sá, S. T. Martin, L. Alexander, B. B. Palm, W. Hu, P. Campuzano-Jost, D. A. Day, J. L.

Jimenez, M. Riva, J. D. Surratt, J. Viegas, A. Manzi, E. Edgerton, K. Baumann, R. Souza, P. Artaxo, and A. H. Goldstein, 2016**,** submitted.

Jacobson, M. Z., 2001: Strong radiative heating due to the mixing state of black carbon in atmospheric aerosols. *Nature*, **409,** 695-697, 10.1038/35055518.

Keller, M., M. Bustamante, J. Gash, and P. Dias, Eds., 2009: *Amazonia and Global Change*. American Geophysical Union.

Khain, A., D. Rosenfeld, and A. Pokrovsky, 2005: Aerosol impact on the dynamics and microphysics of deep convective clouds. *Q. J. R. Meteor.*, **131,** 2639-2663, 10.1256/qj.04.62.

Kuhn, U., L. Ganzeveld, A. Thielmann, T. Dindorf, G. Schebeske, M. Welling, J. Sciare, G. Roberts, F. X. Meixner, J. Kesselmeier, J. Lelieveld, O. Kolle, P. Ciccioli, J. Lloyd, J. Trentmann, P. Artaxo, and M. O. Andreae, 2010: Impact of Manaus city on the Amazon Green Ocean atmosphere: ozone production, precursor sensitivity and aerosol load. *Atmos. Chem. Phys.*, **10,** 9251-9282, 10.5194/acp-10-9251-2010.

Liu, Y., J. Brito, M. R. Dorris, J. C. Rivera-Rios, R. Seco, K. H. Bates, P. Artaxo, S. Duvoisin, F. N. Keutsch, S. Kim, A. H. Goldstein, A. B. Guenther, A. O. Manzi, R. A. F. Souza, S. R. Springston, T. B. Watson, K. A. McKinney, and S. T. Martin, 2016: Isoprene photochemistry over the Amazon rainforest. *Proc. Natl. Acad.,* 10.1073/pnas.1524136113.

Liu, Y. J., I. Herdlinger-Blatt, K. A. McKinney, and S. T. Martin, 2013: Production of methyl vinyl ketone and methacrolein via the hydroperoxyl pathway of isoprene oxidation. *Atmos. Chem. Phys.*, **13,** 5715-5730, 10.5194/acp-13-5715-2013.

Machado, L. A. T., M. A. F. Silva Dias, C. Morales, G. Fisch, D. Vila, R. Albrecht, S. J. Goodman, A. J. P. Calheiros, T. Biscaro, C. Kummerow, J. Cohen, D. Fitzjarrald, E. L. Nascimento, M. S. Sakamoto, C. Cunningham, J.-P. Chaboureau, W. A. Petersen, D. K.

Adams, L. Baldini, C. F. Angelis, L. F. Sapucci, P. Salio, H. M. J. Barbosa, E. Landulfo, R. A. F. Souza, R. J. Blakeslee, J. Bailey, S. Freitas, W. F. A. Lima, and A. Tokay, 2014: The Chuva Project: How Does Convection Vary across Brazil? *B. Am. Meteorol. Soc.*, **95,** 1365-1380, 10.1175/BAMS-D-13-00084.1.

Mares, M. A., 1986: Conservation in South america: problems, consequences, and solutions. *Science*, **233,** 734-739, 10.1126/science.233.4765.734.

Martin, S. T., P. Artaxo, L. A. T. Machado, A. O. Manzi, R. A. F. Souza, C. Schumacher, J. Wang, M. O. Andreae, H. M. J. Barbosa, J. Fan, G. Fisch, A. H. Goldstein, A. Guenther, J. L. Jimenez, U. Pöschl, M. A. Silva Dias, J. N. Smith, and M. Wendisch, 2016: Introduction: Observations and Modeling of the Green Ocean Amazon (GoAmazon2014/5). *Atmos. Chem. Phys.*, **16,** 4785-4797, 10.5194/acp-16-4785-2016.

Martin, S. T., M. O. Andreae, P. Artaxo, D. Baumgardner, Q. Chen, A. H. Goldstein, A. Guenther, C. L. Heald, O. L. Mayol-Bracero, P. H. McMurry, T. Pauliquevis, U. Pöschl, K. A. Prather, G. C. Roberts, S. R. Saleska, M. A. Silva-Dias, D. V. Spracklen, E. Swietlicki, and I. Trebs, 2010a: Sources and Properties of Amazonian Aerosol Particles. *Rev. Geophys.*, **48,** RG2002, 10.1029/2008RG000280.

Martin, S. T., M. O. Andreae, D. Althausen, P. Artaxo, H. Baars, S. Borrmann, Q. Chen, D. K. Farmer, A. Guenther, S. S. Gunthe, J. L. Jimenez, T. Karl, K. Longo, A. Manzi, T. Müller, T. Pauliquevis, M. D. Petters, A. J. Prenni, U. Pöschl, L. V. Rizzo, J. Schneider, J. N. Smith, E. Swietlicki, J. Tota, J. Wang, A. Wiedensohler, and S. R. Zorn, 2010b: An overview of the Amazonian Aerosol Characterization Experiment 2008 (AMAZE-08). *Atmos. Chem. Phys.*, **10,** 11415-11438, 10.5194/acp-10-11415-2010.

Mather, J. H., and J. W. Voyles, 2013: The Arm Climate Research Facility: A Review of Structure and Capabilities. *B. Am. Meteorol. Soc.*, **94,** 377-392, 10.1175/BAMS-D-11-00218.1.

Perring, A. E., S. E. Pusede, and R. C. Cohen, 2013: An Observational Perspective on the Atmospheric Impacts of Alkyl and Multifunctional Nitrates on Ozone and Secondary Organic Aerosol. *Chem. Rev.*, **113,** 5848-5870, 10.1021/cr300520x.

Poschl, U., S. T. Martin, B. Sinha, Q. Chen, S. S. Gunthe, J. A. Huffman, S. Borrmann, D. K. Farmer, R. M. Garland, G. Helas, J. L. Jimenez, S. M. King, A. Manzi, E. Mikhailov, T. Pauliquevis, M. D. Petters, A. J. Prenni, P. Roldin, D. Rose, J. Schneider, H. Su, S. R. Zorn, P. Artaxo, and M. O. Andreae, 2010: Rainforest Aerosols as Biogenic Nuclei of Clouds and Precipitation in the Amazon. *Science*, **329,** 1513-1516, 10.1126/science.1191056.

Rangno, A. L., and P. V. Hobbs, 2005: Microstructures and precipitation development in cumulus and small cumulonimbus clouds over the warm pool of the tropical Pacific Ocean. *Q. J. R. Meteor.*, **131,** 639-673, 10.1256/qj.04.13.

Reutter, P., H. Su, J. Trentmann, M. Simmel, D. Rose, S. S. Gunthe, H. Wernli, M. O. Andreae, and U. Pöschl, 2009: Aerosol- and updraft-limited regimes of cloud droplet formation: influence of particle number, size and hygroscopicity on the activation of cloud condensation nuclei (CCN). *Atmos. Chem. Phys.*, **9,** 7067-7080, 10.5194/acp-9-7067-2009.

Rosenfeld, D., U. Lohmann, G. B. Raga, C. D. O'Dowd, M. Kulmala, S. Fuzzi, A. Reissell, and M. O. Andreae, 2008: Flood or Drought: How Do Aerosols Affect Precipitation? *Science*, **321,** 1309-1313, 10.1126/science.1160606.

Salati, E., and P. B. Vose, 1984: Amazon Basin: A System in Equilibrium. *Science*, **225,** 129-138, 10.1126/science.225.4658.129.

Schmid, B., J. M. Tomlinson, J. M. Hubbe, J. M. Comstock, F. Mei, D. Chand, M. S. Pekour, C. D. Kluzek, E. Andrews, S. C. Biraud, and G. M. McFarquhar, 2014: The DOE ARM Aerial Facility. *B. Am. Meteorol. Soc.*, **95,** 723-742, 10.1175/bams-d-13-00040.1.

Silva Dias, P. L., D. S. Moreira, and G. D. Neto, 2006: The Master Super Model Ensemble System (MSMES). *Eighth International Conference on Southern Hemisphere Meteorology and Oceanography*, Foz do Iguaçu, Brazil, Amer. Meteor. Soc., 1751-1757.

Stokes, G. M., and S. E. Schwartz, 1994: The Atmospheric Radiation Measurement (ARM) Program: Programmatic background and design of the cloud and radiation test bed. *B. Am. Meteorol. Soc.*, **75**, 1201-1221, 10.1175/1520-0477(1994)075<1201:TARMPP>2.0.CO;2.

ter Steege, H., and N. C. Pitman, and D. Sabatier, and C. Baraloto, and R. P. Salomao, and J. E. Guevara, and O. L. Phillips, and C. V. Castilho, and W. E. Magnusson, and J. F. Molino, and A. Monteagudo, and P. Nunez Vargas, and J. C. Montero, and T. R. Feldpausch, and E. N. Coronado, and T. J. Killeen, and B. Mostacedo, and R. Vasquez, and R. L. Assis, and J. Terborgh, and F. Wittmann, and A. Andrade, and W. F. Laurance, and S. G. Laurance, and B. S. Marimon, and B. H. Marimon, Jr., and I. C. Guimaraes Vieira, and I. L. Amaral, and R. Brienen, and H. Castellanos, and D. Cardenas Lopez, and J. F. Duivenvoorden, and H. F. Mogollon, and F. D. Matos, and N. Davila, and R. Garcia-Villacorta, and P. R. Stevenson Diaz, and F. Costa, and T. Emilio, and C. Levis, and J. Schietti, and P. Souza, and A. Alonso, and F. Dallmeier, and A. J. Montoya, and M. T. Fernandez Piedade, and A. Araujo-Murakami, and L. Arroyo, and R. Gribel, and P. V. Fine, and C. A. Peres, and M. Toledo, and C. G. Aymard, and T. R. Baker, and C. Ceron, and J. Engel, and T. W. Henkel, and P. Maas, and P. Petronelli, and J. Stropp, and C. E. Zartman, and D. Daly, and D. Neill, and M. Silveira, and M. R. Paredes, and J. Chave, and A. Lima Filho Dde, and P. M. Jorgensen, and

A. Fuentes, and J. Schongart, and F. Cornejo Valverde, and A. Di Fiore, and E. M. Jimenez, and M. C. Penuela Mora, and J. F. Phillips, and G. Rivas, and T. R. van Andel, and P. von Hildebrand, and B. Hoffman, and E. L. Zent, and Y. Malhi, and A. Prieto, and A. Rudas, and A. R. Ruschell, and N. Silva, and V. Vos, and S. Zent, and A. A. Oliveira, and A. C. Schutz, and T. Gonzales, and M. Trindade Nascimento, and H. Ramirez-Angulo, and R. Sierra, and M. Tirado, and M. N. Umana Medina, and G. van der Heijden, and C. I. Vela, and E. Vilanova Torre, and C. Vriesendorp, and O. Wang, and K. R. Young, and C. Baider, and H. Balslev, and C. Ferreira, and I. Mesones, and A. Torres-Lezama, and L. E. Urrego Giraldo, and R. Zagt, and M. N. Alexiades, and L. Hernandez, and I. Huamantupa-Chuquimaco, and W. Milliken, and W. Palacios Cuenca, and D. Pauletto, and E. Valderrama Sandoval, and L. Valenzuela Gamarra, and K. G. Dexter, and K. Feeley, and G. Lopez-Gonzalez, and M. R. Silman, 2013: Hyperdominance in the Amazonian tree flora. *Science*, **342,** 1243092, 10.1126/science.1243092.

Trebs, I., O. L. Mayol-Bracero, T. Pauliquevis, U. Kuhn, R. Sander, L. Ganzeveld, F. X. Meixner, J. Kesselmeier, P. Artaxo, and M. O. Andreae, 2012: Impact of the Manaus urban plume on trace gas mixing ratios near the surface in the Amazon Basin: Implications for the NO-NO_2-O_3 photostationary state and peroxy radical levels. *J. Geophys. Res.*, **117,** D05307, 10.1029/2011jd016386.

Unger, N., 2012: Global Climate Forcing by Criteria Air Pollutants. *Annual Review of Environment and Resources, Vol 37*, A. Gadgil, and D. M. Liverman, Eds., 1-+.

Valin, L. C., A. R. Russell, and R. C. Cohen, 2013: Variations of OH radical in an urban plume inferred from NO2 column measurements. *Geophys. Res. Lett.*, **40,** 1856-1860, 10.1002/grl.50267.

Wendisch, M., U. Pöschl, M. O. Andreae, L. A. T. Machado, R. Albrecht, H. Schlager, D. Rosenfeld, S. T. Martin, A. Abdelmonem, A. Afchine, A. Araùjo, P. Artaxo, H. Aufmhoff, H. M. J. Barbosa, S. Borrmann, R. Braga, B. Buchholz, M. A. Cecchini, A. Costa, J. Curtius, M. Dollner, M. Dorf, V. Dreiling, V. Ebert, A. Ehrlich, F. Ewald, G. Fisch, A. Fix, F. Frank, D. Fütterer, C. Heckl, F. Heidelberg, T. Hüneke, E. Jäkel, E. Järvinen, T. Jurkat, S. Kanter, U. Kästner, M. Kenntner, J. Kesselmeier, T. Klimach, M. Knecht, R. Kohl, T. Kölling, M. Krämer, M. Krüger, T. C. Krisna, J. V. Lavric, K. Longo, C. Mahnke, A. O. Manzi, B. Mayer, S. Mertes, A. Minikin, S. Molleker, S. Münch, B. Nillius, K. Pfeilsticker, C. Pöhlker, A. Roiger, D. Rose, D. Rosenow, D. Sauer, M. Schnaiter, J. Schneider, C. Schulz, R. A. F. d. Souza, A. Spanu, P. Stock, D. Vila, C. Voigt, A. Walser, D. Walter, R. Weigel, B. Weinzierl, F. Werner, M. A. Yamasoe, H. Ziereis, T. Zinner, and M. Zöger, 2016: The ACRIDICON-CHUVA campaign: Studying tropical deep convective clouds and precipitation over Amazonia using the new German research aircraft HALO. *B. Am. Meteorol. Soc.*, doi:10.1175/BAMS-D-14-00255.1.

Williams, E., D. Rosenfeld, N. Madden, J. Gerlach, N. Gears, L. Atkinson, N. Dunnemann, G. Frostrom, M. Antonio, B. Biazon, R. Camargo, H. Franca, A. Gomes, M. Lima, R. Machado, S. Manhaes, L. Nachtigall, H. Piva, W. Quintiliano, L. Machado, P. Artaxo, G. Roberts, N. Renno, R. Blakeslee, J. Bailey, D. Boccippio, A. Betts, D. Wolff, B. Roy, J. Halverson, T. Rickenbach, J. Fuentes, and E. Avelino, 2002: Contrasting convective regimes over the Amazon: Implications for cloud electrification. *J. Geophys. Res.*, **107,** LBA 50-51-LBA 50-19, 10.1029/2001JD000380.

Yuter, S. E., and R. A. Houze, 1995: Three-Dimensional Kinematic and Microphysical Evolution of Florida Cumulonimbus. Part II: Frequency Distributions of Vertical Velocity,

Reflectivity, and Differential Reflectivity. *Monthly Weather Review*, **123,** 1941-1963, 10.1175/1520-0493(1995)123<1941:TDKAME>2.0.CO;2.

Sidebar 1

Models are used to help understand the effects of human activities on the spatial and temporal variability of important and complex quantities. An example is described here for ozone. Ozone is a secondary trace gas produced by photochemical reactions of nitrogen oxides and volatile organic compounds emitted from anthropogenic and biogenic sources. Exposure to high concentrations of ozone has been shown to be hazardous for human health and cause plant damage. Relatively low ozone concentrations are maintained in the Amazon basin by photochemical production from biogenic emissions, although downward transport during convective events can lead to isolated and rapid increases in surface ozone concentrations. The rate of photochemical production is modulated by the presence of clouds that frequently occur. During the dry season, biomass burning releases additional precursor gases that further enhance ozone production. Ozone is removed from the atmosphere by dry deposition on plant surfaces. Daily maximum ozone concentrations are usually between 10 and 20 ppb during the wet season under background conditions, but values as high as 100 ppb have been observed during the dry season in the presence of biomass burning. Pollutants emitted from Manaus perturb the background atmosphere of the tropical rain forest and react with volatile organic compounds emitted from the forest. The figure (:: Figure Sidebar 1 here ::) shows an example simulation from the Weather Research and Forecasting (WRF)-Chem model of ozone mixing ratios downwind of Manaus for March 13, 2014. Based on the G-1 measurements, the observed plume centerline passed over the T2 and T3 sites on this day. Although the plume centerline of the model is north of the observed centerline location due to errors in the simulated wind direction, the concentrations are similar to the observations as shown in Figure 5a. The model demonstrates that anthropogenic emissions influence chemical reactions over the rainforest far downwind of

Manaus, such as depleting isoprene emitted by the forest. Modeling helps to better anticipate possible future impacts of climate change and population increases in the Amazon basin and other tropical regions of the world.

Sidebar 2

The lifetime of many species in the atmosphere depends on the reaction rate with hydroxyl radical (OH). Elevated NO_x concentrations in the pollution plume of Manaus can increase the rate of OH radical production and hence the steady-state concentration of OH radicals. As a result, the oxidation cycle can become accelerated, meaning that the concentrations of parent species decrease and the concentrations of product species increase because of the higher OH concentrations. One specific example highlighted in this article is the decreased concentrations of isoprene and the increased concentrations of its daughter species methyl vinyl ketone and methacrolein (Figures 5b and 5c). Direct measurements of OH radical concentrations were also made at the T3 ground site, and the accelerating effect of the pollution plume can be directly resolved. As seen in the accompanying figure, on March 14, 2014, there was an abrupt shift at 16:00 (UTC) in particle counts (scaled from 0 to 12000 cm^{-3}) and ozone concentrations (scaled from 0 to 60 ppb) (:: Figure Sidebar 2 here ::). This shift corresponded to a change in local winds from easterlies, which carried the Manaus plume, to southerlies, which transported background air. Because the hydroxyl radical has a lifetime of less than 1 s, the measured OH concentrations are specifically representative of each air mass. For similar solar irradiation, the hydroxyl radical concentration increased by a factor of more than three for polluted compared to background air.

List of Figures

These results are produced by the MASTER-IAG model using a combination of data assimilation from the GFS-NCEP at 0.5° resolution and numerical modeling with BRAMS at 2-km resolution of forward trajectories launched over Manaus ("T1") (Silva Dias et al. 2006; Freitas et al. 2009). Abbreviations: MASTER-IAG, Meteorologia Aplicada a Sistemas de Tempo Regionais - Instituto de Astronomia, Geofísica e Ciências Atmosféricas, http://www.master.iag.usp.br/; GFS-NCEP, Global Forecast System - National Centers for Environmental Prediction, GFS-NCEP, http://www.nco.ncep.noaa.gov/pmb/products/gfs/; BRAMS, Brazilian developments on the Regional Atmospheric Modelling System, http://brams.cptec.inpe.br/. All sites accessed 3 January 2016.

Figure 3. The GoAmazon2014/5 experiment in pictures. (top, left) The verdant Amazon rain forest forming a green ocean, as observed from the top of the research tower at T0k. (top, right) Photo of G-1 aircraft taken when flying in formation with the HALO aircraft. Compared to the G-1 that mostly sampled regionally around Manaus with a focus on the pollution plume, the HALO aircraft mostly observed the free troposphere across a larger part of the Amazon basin. Those observations are described in a complementary article by Wendisch et al. (2016). (center) Yellow pins indicate the of GoAmazon2014/5 research sites in the environs of the city of Manaus (-3.1°, -60.0°) in the state of Amazonas in the country of Brazil. The ground sites include upwind locations (T0a, T0e, T0k, and T0t), source location (T1), and downwind locations (T2, T3, and T3u) (Martin et al. 2016). Site T0a is the Amazonian Tall Tower Observatory (ATTO) described by Andreae et al. (2015). Manaus sits at the confluence of Rio Negro and Rio Solimões, where the named Rio Amazonas begins

(Portuguese names). The inset shows the location of the experimental domain within South America. For prevailing winds, Manaus is on order 1200 km from the Atlantic Ocean during the wet season and 1600 km during the dry season. (bottom, left) Aerial view of the research containers at the T3 research site. This site was administered by the Atmospheric Radiation Measurement (ARM) Climate Research Facility, a user facility of the United States Department of Energy (Mather and Voyles 2013), in collaboration with Brazilian National Institute of Amazonian Research (INPA). (bottom, right) Ground-level shot highlighting two of the radar systems at T3.

Figure 4. Visualization of the Manaus pollution plume. In the left-hand panel, the direction and extent of the plume observed in the Manaus environs by the G-1 aircraft is represented by plotting particle number concentrations in the vertical axis. In the right-hand panel, several tracers of the pollution plume, especially as related to air quality, are plotted. In the right-hand plots, the abscissa represents position along the flight path represented in the left-hand plots. (a1) Particle concentrations recorded by a condensation particle counter (CPC; TSI Model 3025A) on board the G-1 aircraft on a flight track at 500 m above sea level (asl) from 14:15to 15:33 (UTC) on March 13, 2014, corresponding to local time of 10:15 to 11:33. Local topography varies from 50 to 100 m (asl). The figure shows an image of the local land cover upon which relative particle concentrations along the flight track are plotted in the vertical axis in blue coloring. The flight track was transverse to the Manaus pollution plume. Yellow pins indicate the locations of some of the GoAmazon2014/5 research sites (cf. Figure 3). The yellow line shows the simulated trajectory of an air parcel released over Manaus at 500 m (asl). (a2) Time series of concentrations of particles, carbon

monoxide, and oxides of nitrogen along the flight track of panel a1. Time zero corresponds to 15:33 (UTC). For particle concentrations, the black and gray traces correspond to particles of 3 nm and larger and 10 nm and larger, respectively, using two different condensation particle counters (TSI Models 3025A and 3010, respectively). For concentrations of oxides of nitrogen, the black and gray traces correspond to concentrations of NO_2 and NO, respectively. The red line represents concentrations recorded in background air masses during the flight and thus represents a baseline against which to measure the effects of pollution on species concentrations. The designation "T3" at 3088 s indicates the time point at which the G-1 aircraft was located over the T3 research site. Background coloring designates that the G-1 was passing through a background air mass (light green), a polluted air mass (light red), or an air mass having an undetermined pollution state (light orange). The classification algorithm took as input the concentrations of particles, carbon monoxide, and oxides of nitrogen. (b1) Particles concentrations recorded on the same flight as panel a1 at 500 m (asl) but from 15:39:00 to 15:54:00 (UTC), corresponding to local time of 11:39 to 11:54. The flight track was longitudinal to the Manaus pollution plume. (b2) Time series of species concentrations along the flight track of panel b2. Although the actual flight was upwind, to visualize as downwind translation from Manaus, time is expressed in reverse flight time. Hence, time zero corresponds to 15:54 (UTC). Trace coloring is as for panel a2. Reported concentrations are normalized to standard temperature and pressure (STP; 10^5 Pa, 273.15 K).

Figure 5. Concentrations of atmospheric gases along the transverse flight tracks of panels a1 and a2 of Figure 4: (a) ozone, (b) isoprene, (c) ratio of oxidation products to isoprene,

and (d) ratio of benzene to toluene. The data sets reveal the acceleration of the oxidant cycle inside compared to outside the plume downwind of Manaus (cf. main text). Isoprene oxidation products include methyl vinyl ketone, methacrolein, and hydroperoxides. Organic species were measured by proton-transfer-reaction mass spectrometry (PTR-MS). The background coloring to designate the pollution state of an air mass, the red line to designate baseline concentrations, and the label "T3" are as discussed for panel a2 of Figure 4.

Figure 6. Properties of cloud condensation nuclei (CCN) along the transverse flight corresponding to panel a1 of Figure 4. The data sets show that the cloud-forming characteristics of the atmospheric PM were altered by the pollution plume. (a) CCN concentrations measured at 0.23% supersaturation, (b) CCN concentrations measured at 0.5% supersaturation, (c) total particle concentration of diameters of 100 nm and larger, (d) fraction of CCN-active particles calculated as the ratio of CCN concentrations at 0.23% to total particle concentrations of diameters of 100 nm and larger, (e) fraction of CCN-active particles calculated as the ratio of CCN concentrations at 0.23% to total particle concentrations of diameters of 10 nm and larger. The background coloring to designate the pollution state of an air mass, the red line to designate baseline concentrations, and the label "T3" are as discussed for panel a2 of Figure 4.

Figure 7. Droplet size distributions of clouds under polluted and background conditions. The microphysical cloud properties in the regions affected by the Manaus plume are significantly different. (top) CCN concentrations at 0.35% supersaturation along a flight track on March 19, 2014, that passed through clouds under background

conditions (blue line) and along a flight track on March 21, 2014, that transected the Manaus pollution plume several times while passing through clouds (red line). Time on the abscissa runs from 17:00 to 18:00 UTC for March 21 (polluted) and from 14:40 to 15:20 UTC for March 19 (background). (btm) Droplet size distributions for clouds during the polluted and background conditions represented by the top panel. The ordinate represents the differential concentration divided by the differential change in $\log_{10}$ diameter. The distributions were prepared by concatenating the data recorded by the Cloud Droplet Probe (CDP), the Two-Dimensional Stereo Probe (2DS), and the High Volume Precipitation Spectrometer, Version 3 (HVPS-3). CDP data were used for sizes <20.0 μm; 2DS and CDP data were averaged for 20.0 to 50.0 μm; 2DS data were used for 50.0 to 100.0 μm; and HVPS data were used for >100 μm. For the polluted case, data were filtered to include measurements having CCN concentrations of 300 cm^{-3} and greater so as to consider only clouds inside the Manaus plume.

Figure 8. Vertical distributions of the frequency radar reflectivity over site T3 during IOP1 in the wet season. In statistical aggregate, the pollution plume downwind of Manaus appears to alter cloud properties. The shown plots are commonly referred to as a "Contoured Frequency by Altitude Diagram" (CFAD), as introduced by Yuter and Houze (1995). The top and bottom panels show data segregated by polluted and background conditions, respectively. Inset lines accompany the description in the text to demarcate a height of 5 km and a reflectivity range of 15 to 20 dBZ. The data were collected in a vertical pointing strategy by a dual polarization X-band scanning radar (Machado et al. 2014).

Figure 9. Segregation of rain rate and mean mass-weighted droplet diameter by polluted or background conditions. A mixture of influences affects rainfall occurrence and intensity, and at times pollution can play a role in shifting the kinematic and microphysical growth processes. Data points in the figure represent rainfall intervals of 5 min. Measurements were made by a disdrometer at T3. A data threshold was used of a rain rate greater than 0.5 mm h^{-1} and a droplet count above 50.

List of Sidebar Figures

These figures are in low resolution for following procedures of BAMS for review. High-resolution figures are available for publication.

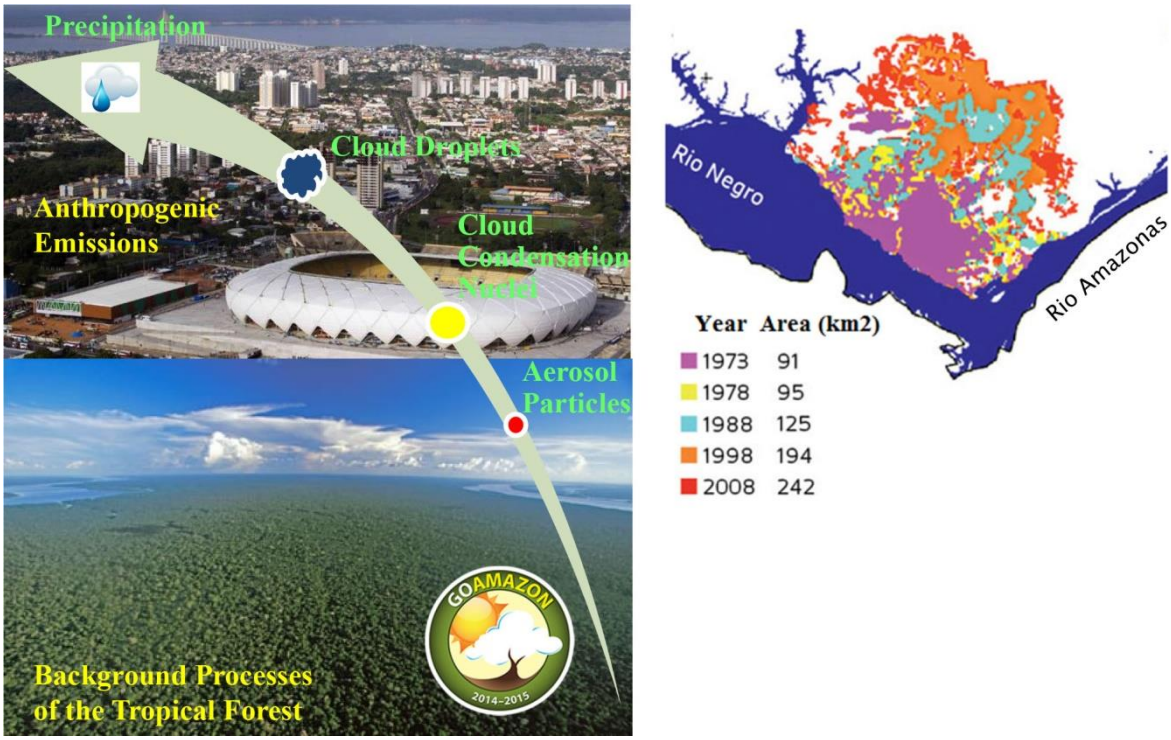

Figure 1. The GoAmazon2014/5 experiment in concept. The left panel represents the advection by wind of a background air mass into Manaus, emissions into this air mass while over the city, and the transformation of atmospheric species as the air mass continues downwind of the urban region. The air mass is laden with biogenic volatile organic carbon compounds (BVOCs) emitted by the forest both upwind and downwind of the city. These BVOCs are transformed by the atmospheric oxidant cycle into aerosol particles. The prevailing chemical reactions are altered by pollution. The particulate matter serves as cloud condensation nuclei (CCN). As a result, cloud properties and possibly rainfall can be modified in response to different levels of pollution over the tropical rain forest. As a surrogate for scaled anthropogenic emissions, the right panel shows the expansion of the urban region of Manaus (-3.1°, -60.0°), Brazil, across four decades. The right-side image is adapted from http://revistapesquisa.fapesp.br/wp-content/uploads/2012/10/078-081_ilhascalor_200.pdf, accessed 11 August 2015.

These figures are in low resolution for following procedures of BAMS for review. High-resolution figures are available for publication.

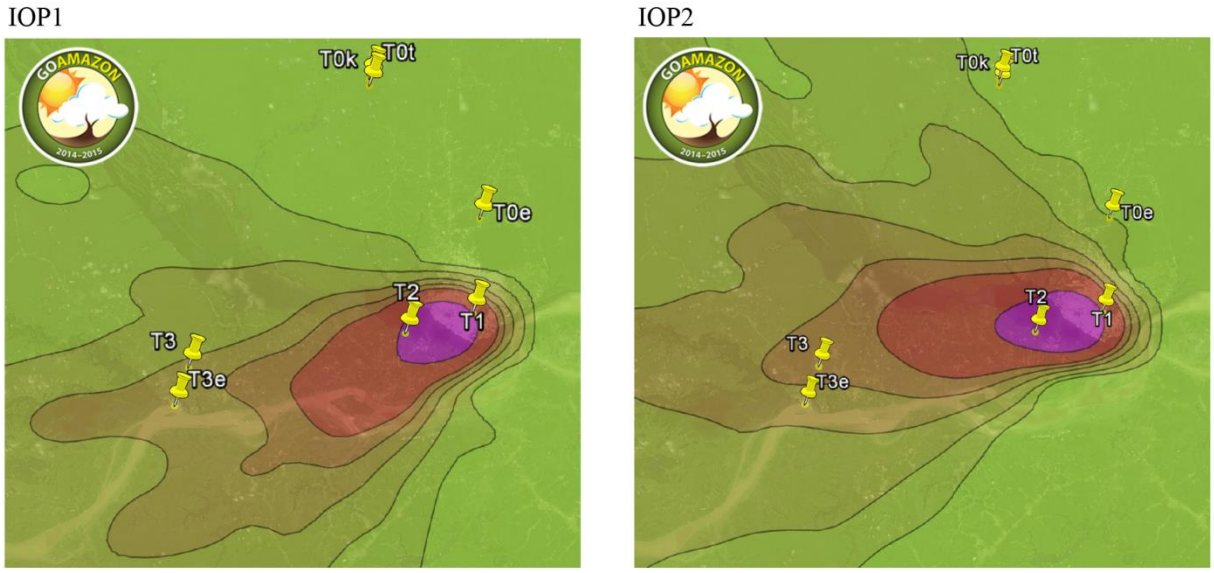

Figure 2. Statistical composite of forward trajectories launched 500 m above site "T1" in Manaus at 00, 06, 12, and 18 UTC for (left) the 59 days of IOP1 and (right) the 60 days of IOP2. Easterlies associated with trade winds normally swept the urban pollution plume westward toward the downwind research sites. The intensity of the contour coloring represents the frequency for trajectories that passed nearby the latitude/longitude position represented by the map. Contours are drawn at 2%, 5%, 10%, 15%, 20%, and 40% frequency on a grid size of 0.1° × 0.1°. Yellow pins show the locations of some of the GoAmazon2014/5 research sites (cf. Figure 3). These results are produced by the MASTER-IAG model using a combination of data assimilation from the GFS-NCEP at 0.5° resolution and numerical modeling with BRAMS at 2-km resolution of forward trajectories launched over Manaus ("T1") (Silva Dias et al. 2006; Freitas et al. 2009). Abbreviations: MASTER-IAG, Meteorologia Aplicada a Sistemas de Tempo Regionais - Instituto de Astronomia, Geofísica e Ciências Atmosféricas, http://www.master.iag.usp.br/; GFS-NCEP, Global Forecast System - National Centers for Environmental Prediction, GFS-NCEP, http://www.nco.ncep.noaa.gov/pmb/products/gfs/; BRAMS, Brazilian developments on the Regional Atmospheric Modelling System, http://brams.cptec.inpe.br/. All sites accessed 3 January 2016.

These figures are in low resolution for following procedures of BAMS for review. High-resolution figures are available for publication.

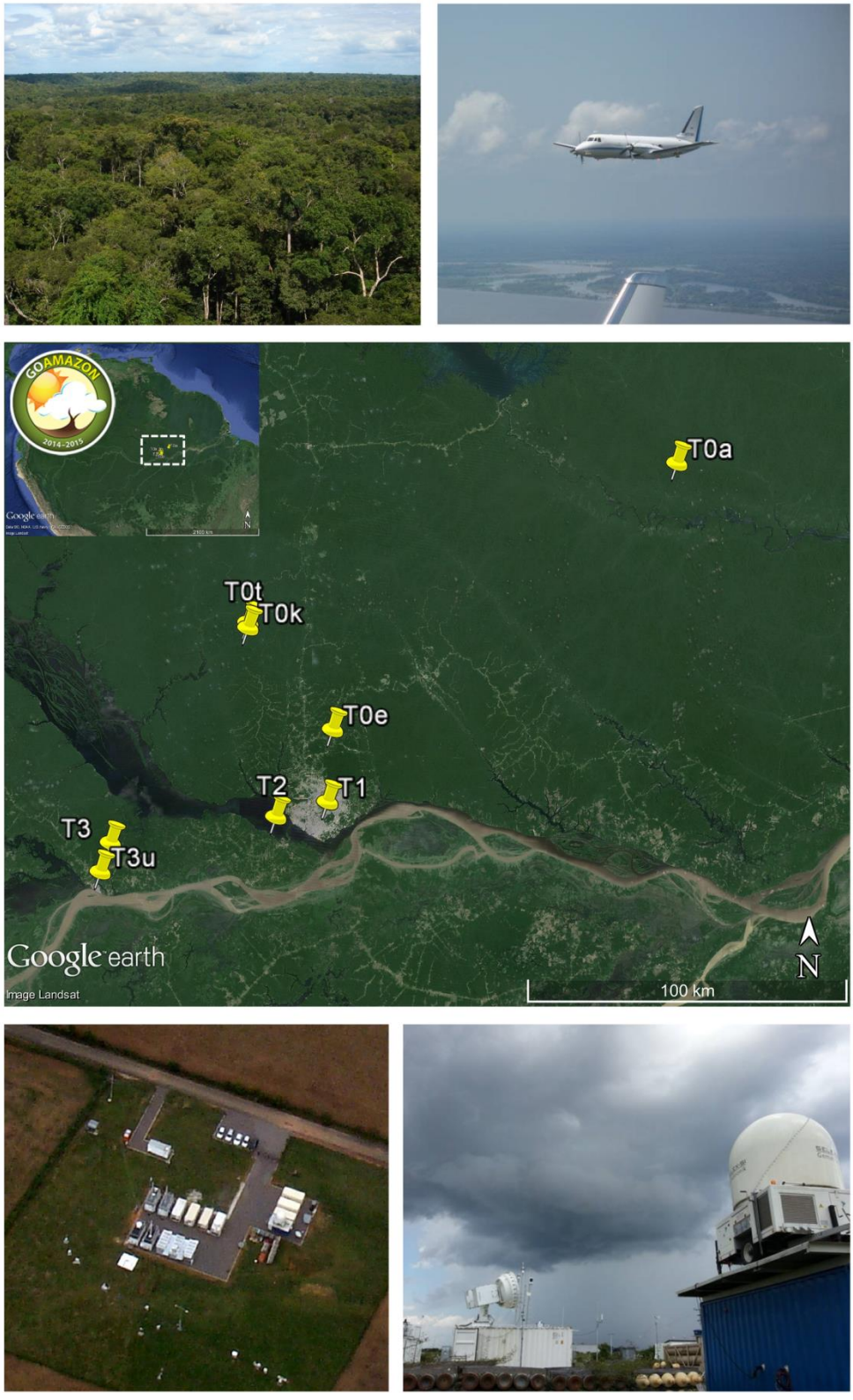

Figure 3. The GoAmazon2014/5 experiment in pictures. (top, left) The verdant Amazon rain forest forming a green ocean, as observed from the top of the research tower at T0k. (top, right) Photo of G-1 aircraft taken when flying in formation with the HALO aircraft. Compared to the G-1 that mostly sampled

These figures are in low resolution for following procedures of BAMS for review. High-resolution figures are available for publication.

regionally around Manaus with a focus on the pollution plume, the HALO aircraft mostly observed the free troposphere across a larger part of the Amazon basin. Those observations are described in a complementary article by Wendisch et al. (2016). (center) Yellow pins indicate the locations of GoAmazon2014/5 research sites in the environs of the city of Manaus (-3.1°, -60.0°) in the state of Amazonas in the country of Brazil. The ground sites include upwind locations (T0a, T0e, T0k, and T0t), source location (T1), and downwind locations (T2, T3, and T3u) (Martin et al. 2016). Site T0a is the Amazonian Tall Tower Observatory (ATTO) described by Andreae et al. (2015). Manaus sits at the confluence of Rio Negro and Rio Solimões, where the named Rio Amazonas begins (Portuguese names). The inset shows the location of the experimental domain within South America. For prevailing winds, Manaus is on order 1200 km (IOP1) to 1600 km (IOP2) from the Atlantic Ocean. (bottom, left) Aerial view of the research containers at the T3 research site. This site was administered by the Atmospheric Radiation Measurement (ARM) Climate Research Facility, a user facility of the United States Department of Energy (Mather; Voyles 2013), in collaboration with Brazilian National Institute of Amazonian Research (INPA). (bottom, right) Ground-level shot highlighting two of the radar systems at T3.

These figures are in low resolution for following procedures of BAMS for review. High-resolution figures are available for publication.

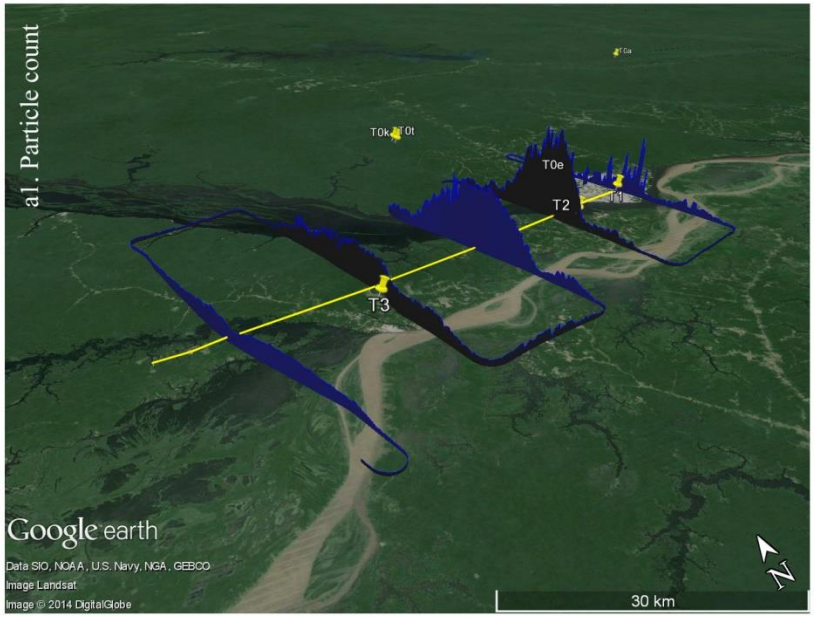

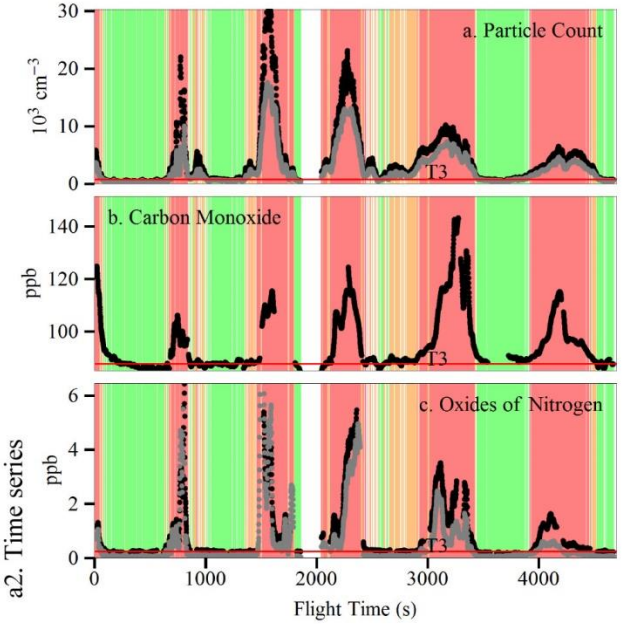

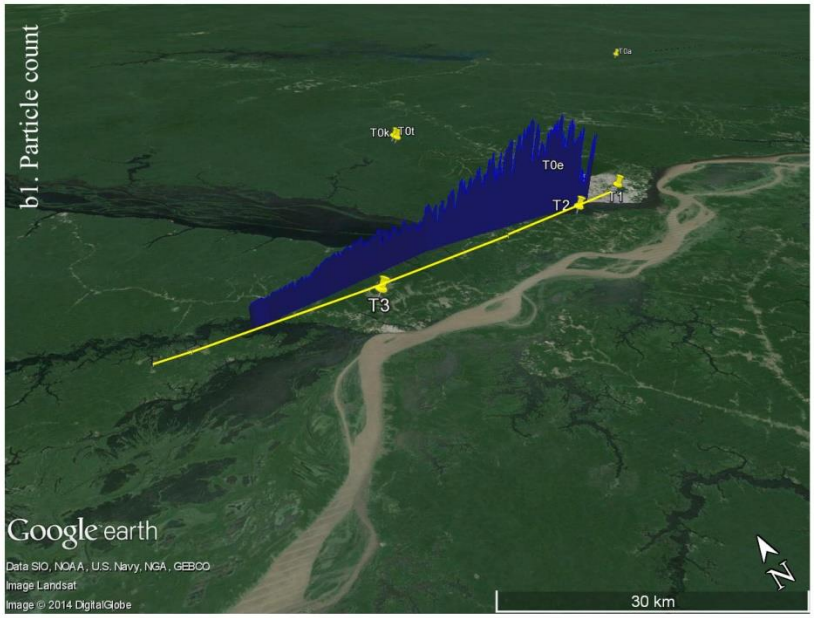

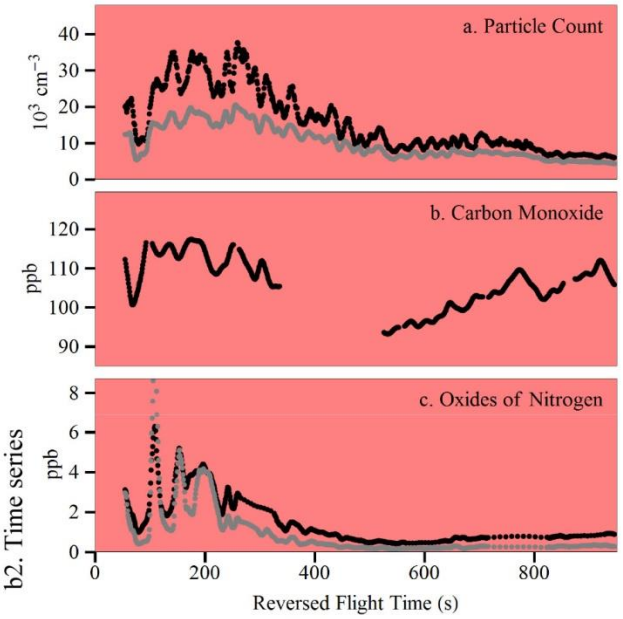

These figures are in low resolution for following procedures of BAMS for review. High-resolution figures are available for publication.

Figure 4. Visualization of the Manaus pollution plume. In the left-hand panel, the direction and extent of the plume observed in the Manaus environs by the G-1 aircraft is represented by plotting particle number concentrations in the vertical axis. In the right-hand panel, several tracers of the pollution plume, especially as related to air quality, are plotted. In the right-hand plots, the abscissa represents position along the flight path represented in the left-hand plots. (a1) Particle concentrations recorded by a condensation particle counter (CPC; TSI Model 3025A) on board the G-1 aircraft on a flight track at 500 m above sea level (asl) from 14:15to 15:33 (UTC) on March 13, 2014, corresponding to local time of 10:15 to 11:33. Local topography varies from 50 to 100 m (asl). The figure shows an image of the local land cover upon which relative particle concentrations along the flight track are plotted in the vertical axis in blue coloring. The flight track was transverse to the Manaus pollution plume. Yellow pins indicate the locations of some of the GoAmazon2014/5 research sites (cf. Figure 3). The yellow line shows the simulated trajectory of an air parcel released over Manaus at 500 m (asl). (a2) Time series of concentrations of particles, carbon monoxide, and oxides of nitrogen along the flight track of panel a1. Time zero corresponds to 15:33 (UTC). For particle concentrations, the black and gray traces correspond to particles of 3 nm and larger and 10 nm and larger, respectively, using two different condensation particle counters (TSI Models 3025A and 3010, respectively). For concentrations of oxides of nitrogen, the black and gray traces correspond to concentrations of NO_2 and NO, respectively. The red line represents concentrations recorded in background air masses during the flight and thus represents a baseline against which to measure the effects of pollution on species concentrations. The designation "T3" at 3088 s indicates the time point at which the G-1 aircraft was located over the T3 research site. Background coloring designates that the G-1 was passing through a background air mass (light green), a polluted air mass (light red), or an air mass having an undetermined pollution state (light orange). The classification algorithm took as input the concentrations of particles, carbon monoxide, and oxides of nitrogen. (b1) Particles concentrations recorded on the same flight as panel a1 at 500 m (asl) but from 15:39:00 to 15:54:00 (UTC), corresponding to local time of 11:39 to 11:54. The flight track was longitudinal to the Manaus pollution plume. (b2) Time series of species concentrations along the flight track of panel b2. Although the actual flight was upwind, to visualize as downwind translation from Manaus, time is expressed in reverse flight time. Hence, time zero corresponds to 15:54 (UTC). Trace coloring is as for panel a2. Reported concentrations are normalized to standard temperature and pressure (STP; 10^5 Pa, 273.15 K).

These figures are in low resolution for following procedures of BAMS for review. High-resolution figures are available for publication.

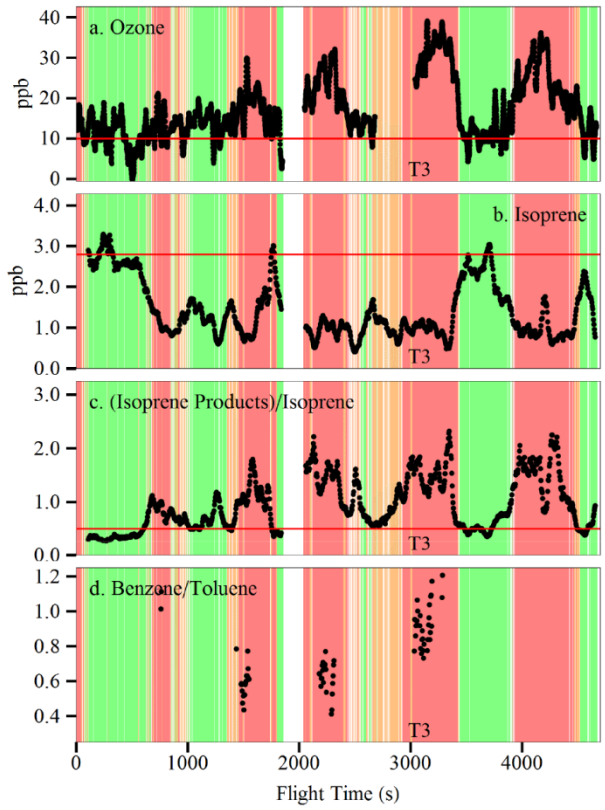

Figure 5. Concentrations of atmospheric gases along the transverse flight tracks of panels a1 and a2 of Figure 4: (a) ozone, (b) isoprene, (c) ratio of oxidation products to isoprene, and (d) ratio of benzene to toluene. The data sets reveal the acceleration of the oxidant cycle inside compared to outside the plume downwind of Manaus (cf. main text). Isoprene oxidation products include methyl vinyl ketone, methacrolein, and hydroperoxides. Organic species were measured by proton-transfer-reaction mass spectrometry (PTR-MS). The background coloring to designate the pollution state of an air mass, the red line to designate baseline concentrations, and the label "T3" are as discussed for panel a2 of Figure 4.

These figures are in low resolution for following procedures of BAMS for review. High-resolution figures are available for publication.

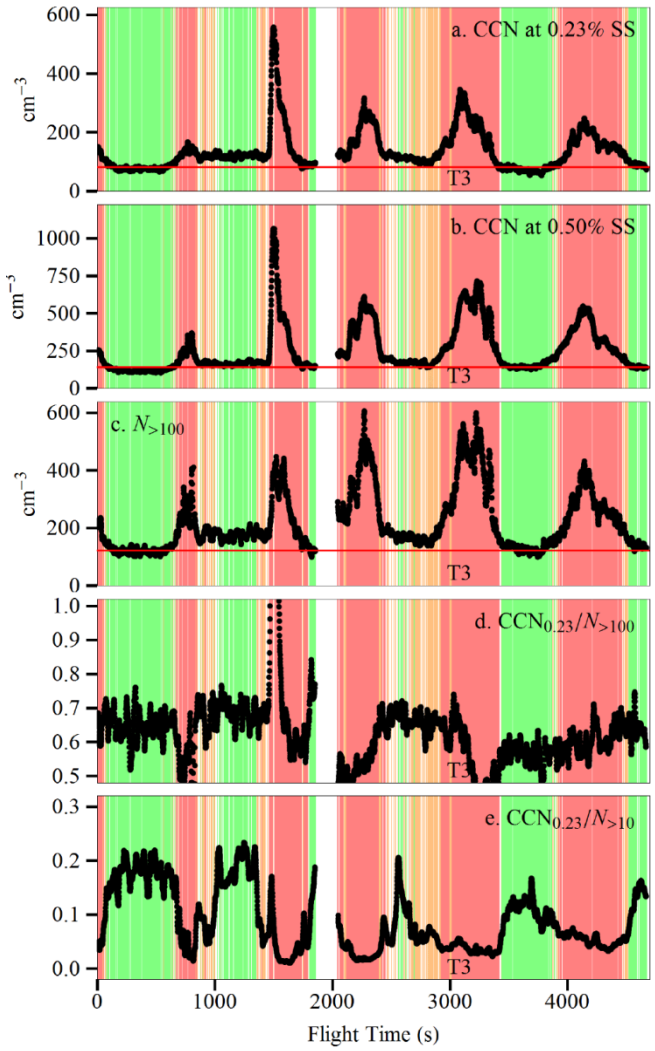

Figure 6. Properties of cloud condensation nuclei (CCN) along the transverse flight corresponding to panel a1 of Figure 4. The data sets show that the cloud-forming characteristics of the atmospheric PM were altered by the pollution plume. (a) CCN concentrations measured at 0.23% supersaturation, (b) CCN concentrations measured at 0.5% supersaturation, (c) total particle concentration of diameters of 100 nm and larger, (d) fraction of CCN-active particles calculated as the ratio of CCN concentrations at 0.23% to total particle concentrations of diameters of 100 nm and larger, (e) fraction of CCN-active particles calculated as the ratio of CCN concentrations at 0.23% to total particle concentrations of diameters of 10 nm and larger. The background coloring to designate the pollution state of an air mass, the red line to designate baseline concentrations, and the label "T3" are as discussed for panel a2 of Figure 4.

These figures are in low resolution for following procedures of BAMS for review. High-resolution figures are available for publication.

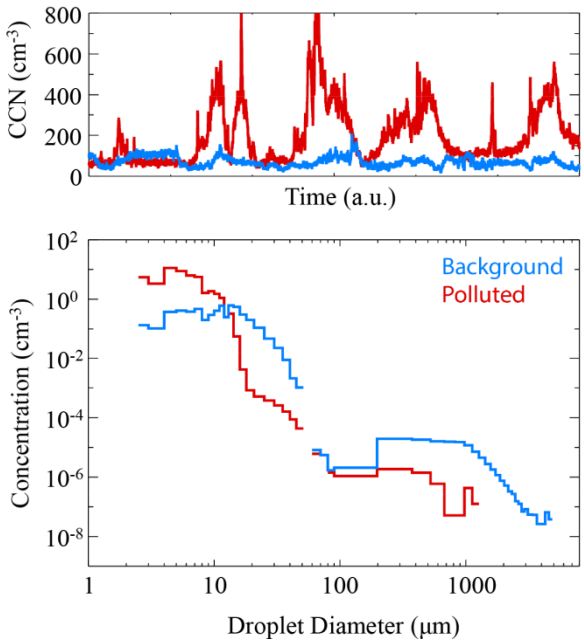

Figure 7. Droplet size distributions of clouds under polluted and background conditions. The microphysical cloud properties in the regions affected by the Manaus plume are significantly different. (top) CCN concentrations at 0.35% supersaturation along a flight track on March 19, 2014, that passed through clouds under background conditions (blue line) and along a flight track on March 21, 2014, that transected the Manaus pollution plume several times while passing through clouds (red line). Time on the abscissa runs from 17:00 to 18:00 UTC for March 21 (polluted) and from 14:40 to 15:20 UTC for March 19 (background). (btm) Droplet size distributions for clouds during the polluted and background conditions represented by the top panel. The ordinate represents the differential concentration divided by the differential change in $\log_{10}$ diameter. The distributions were prepared by concatenating the data recorded by the Cloud Droplet Probe (CDP), the Two-Dimensional Stereo Probe (2DS), and the High Volume Precipitation Spectrometer, Version 3 (HVPS-3). CDP data were used for sizes <20.0 μm; 2DS and CDP data were averaged for 20.0 to 50.0 μm; 2DS data were used for 50.0 to 100.0 μm; and HVPS data were used for >100 μm. For the polluted case, data were filtered to include measurements having CCN concentrations of 300 cm^{-3} and greater so as to consider only clouds inside the Manaus plume.

These figures are in low resolution for following procedures of BAMS for review. High-resolution figures are available for publication.

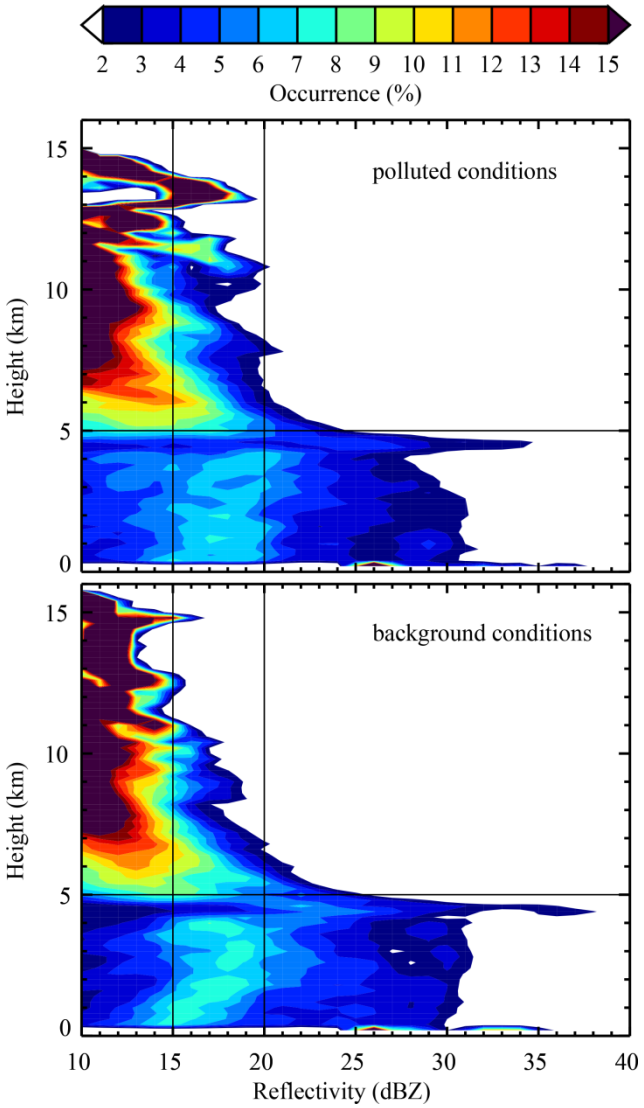

Figure 8. Vertical distributions of the frequency radar reflectivity over site T3 during IOP1 in the wet season. In statistical aggregate, the pollution plume downwind of Manaus appears to alter cloud properties. The shown plots are commonly referred to as a "Contoured Frequency by Altitude Diagram" (CFAD), as introduced by Yuter and Houze (1995). The top and bottom panels show data segregated by polluted and background conditions, respectively. Inset lines accompany the description in the text to demarcate a height of 5 km and a reflectivity range of 15 to 20 dBZ. The data were collected in a vertical pointing strategy by a dual polarization X-band scanning radar (Machado et al. 2014).

These figures are in low resolution for following procedures of BAMS for review. High-resolution figures are available for publication.

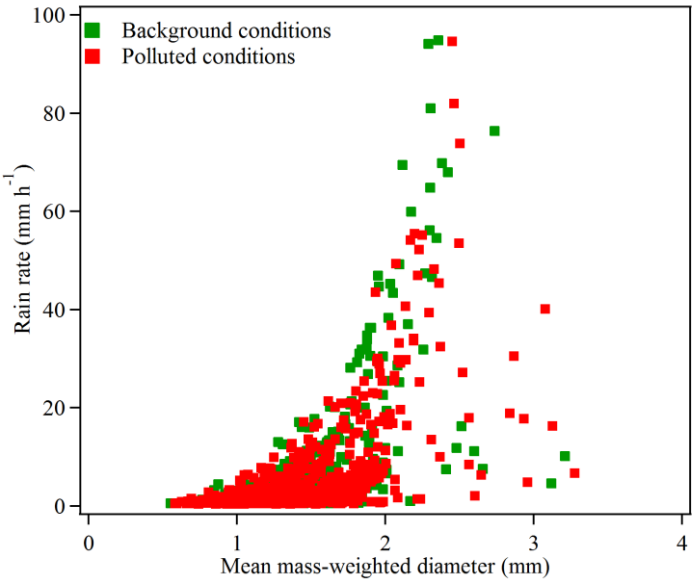

Figure 9. Segregation of rain rate and mean mass-weighted droplet diameter by polluted or background conditions. A mixture of influences affects rainfall occurrence and intensity, and at times pollution can play a role in shifting the kinematic and microphysical growth processes. Data points in the figure represent rainfall intervals of 5 min. Measurements were made by a disdrometer at T3. A data threshold was used of a rain rate greater than 0.5 mm h^{-1} and a droplet count above 20.

These figures are in low resolution for following procedures of BAMS for review. High-resolution figures are available for publication.

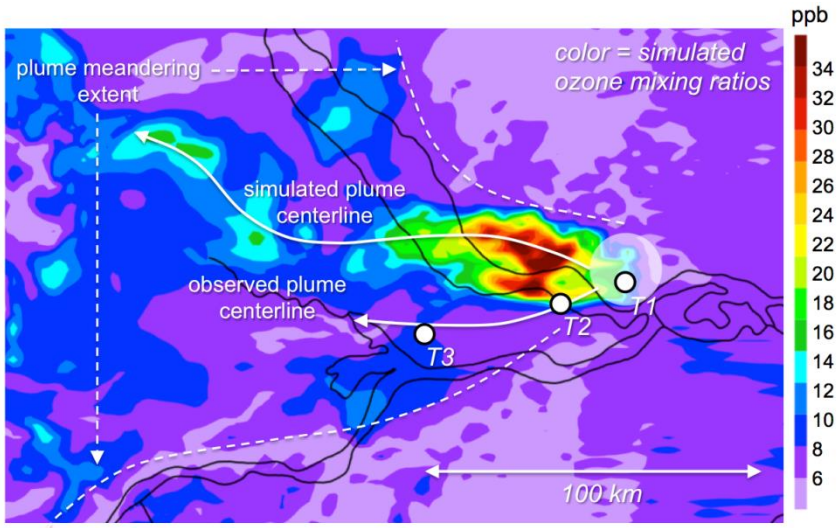

Figure SB1. Modeling the urban pollution plume.

These figures are in low resolution for following procedures of BAMS for review. High-resolution figures are available for publication.

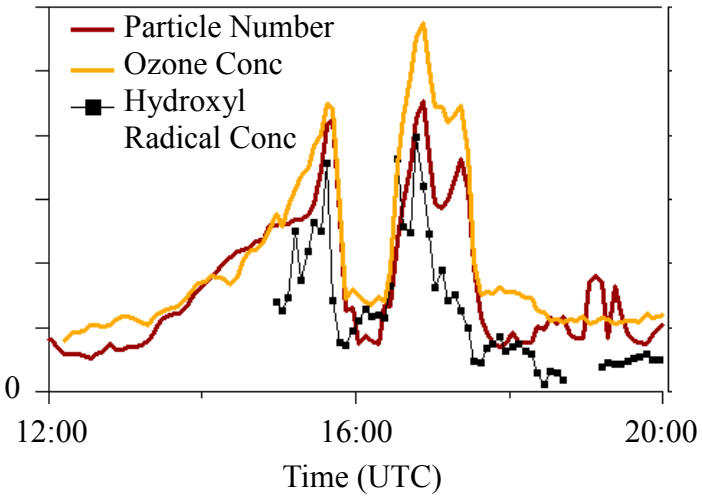

Figure SB2. The accelerated oxidant cycle.